



HAL
open science

Searching For Many-body Effects And Efimov States In Very Weakly Bound Triatomics: HeNeH⁻ And HeNeH.

F Gianturco, Sergio Orlandini, Isabella Baccarelli

► **To cite this version:**

F Gianturco, Sergio Orlandini, Isabella Baccarelli. Searching For Many-body Effects And Efimov States In Very Weakly Bound Triatomics: HeNeH⁻ And HeNeH.. *Molecular Physics*, 2008, 106 (02-04), pp.573-586. 10.1080/00268970801939001 . hal-00513178

HAL Id: hal-00513178

<https://hal.science/hal-00513178>

Submitted on 1 Sep 2010

HAL is a multi-disciplinary open access archive for the deposit and dissemination of scientific research documents, whether they are published or not. The documents may come from teaching and research institutions in France or abroad, or from public or private research centers.

L'archive ouverte pluridisciplinaire **HAL**, est destinée au dépôt et à la diffusion de documents scientifiques de niveau recherche, publiés ou non, émanant des établissements d'enseignement et de recherche français ou étrangers, des laboratoires publics ou privés.



Searching For Many-body Effects And Efimov States In Very Weakly Bound Triatomics: HeNeH⁻ And HeNeH.

Journal:	<i>Molecular Physics</i>
Manuscript ID:	TMPH-2007-0305.R2
Manuscript Type:	Full Paper
Date Submitted by the Author:	22-Jan-2008
Complete List of Authors:	Gianturco, F; University of Rome, chemistry orlandini, sergio; Univerisy of Rome 1, chemistry Baccarelli, Isabella; CASPUR, super computing consortium
Keywords:	van der waals systems, triatomic complexes, weakly bound states
<p>Note: The following files were submitted by the author for peer review, but cannot be converted to PDF. You must view these files (e.g. movies) online.</p> <p>3BHeNeH.tex</p>	



1
2
3 SEARCHING FOR MANY-BODY EFFECTS AND EFIMOV
4
5 STATES IN VERY WEAKLY BOUND TRIATOMICS: HeNeH⁻
6
7
8 AND HeNeH. *
9

10 S. Orlandini⁺, I. Baccarelli[‡], F.A. Gianturco^{+ †}

11
12 ⁺*Department of Chemistry and CNISM,*

13
14 *University of Rome La Sapienza, Piazzale A. Moro 5, 00185 Rome, Italy*

15
16 [‡]*CASPUR, Supercomputing Consortium, via dei Tizii 6, 00185 Rome, Italy*
17

18
19 Abstract

20
21 The rotationless, vibrational states of two weakly bound triatomic species are calculated using
22 a variational expansion over multicentered Gaussian functions (the DGF method described in the
23 main text) and corrections are introduced by using the three-body potentials *vis à vis* the sum-
24 of-potentials approximation. The effects are seen to be very small and isotopic substitution is
25 further introduced to evaluate changes on the vibrational structures of both systems, aiming at
26 possibly detecting Efimov behaviour in such special trimers: no Efimov states are found with the
27 available potentials and when the two-body potential strengths are varied. An additional study on
28 the effects of isotopic substitutions for H atoms is also presented.
29
30
31
32
33
34
35
36
37
38
39
40
41
42
43
44
45
46
47
48
49
50
51
52
53
54
55
56

57
58 * This paper is dedicated to Professor R.D. Levine, a great scientist and a dear friend, on the occasion of
59 his 70th birthday.

60 † Corresponding author; e.mail address: fa.gianturco@caspur.it; fax: +39.06.49913305.

I. INTRODUCTION

The detailed understanding of the complexity of the few-body energy spectra has been the subject of numerous theoretical and experimental studies since the early days of quantum mechanics.

Already in the early thirties L. Thomas [1] predicted that three particles may become effectively bound even when their pairwise interactions support a single, and very weakly bound, state: a result later generalized by Efimov [2] who predicted that the number of bound states of three identical bosons increases to infinity when the pairwise, two-body (2B) potential is weakened so much that the 2B bound state supported by it ceases to exist. Such a new sequence of excited states has therefore been called the Efimov effect, a special feature which makes the sequence to disappear into the three-body (3B) continuum as the 2B interaction is strengthened once more in its attractive part.

The possibility of manipulating low-energy interatomic forces by using magnetically tunable Fano-Feshbach resonances has brought about new perspectives for the study, and possible observation, of the Efimov scenario since the experiments with cold gases of both Fermionic and Bosonic species [3–7] have demonstrated that adiabatic sweeps of the magnetic field strength can be used to associate highly excited Feshbach molecules with an arbitrary weak bond strength.

It is therefore fairly evident that to be able to reliably carry out any numerical experiment on three-particle structures in very weakly bound systems, one needs to start with a correspondingly reliable knowledge of at least the underlying 2B, pairwise potentials and to set up a computational procedure which can robustly generate the final bound states of the trimer of interest.

In other words, the detailed study of general trimers of nonidentical particles which support either only one or very few bound states is of direct interest for covering the necessary background knowledge on the behaviour of very weakly bound complexes and on the sensitivity of the features of the adopted potential in providing evidence for possible Efimov effects in those systems [8].

An outline of the approach for obtaining reliable structures for a chosen candidate system could therefore proceed as follows: (i) one selects a set of pairwise potentials between the three particles which constitute the complex, be it of either identical or different partners;

1
2
3 (ii) decide to describe the overall interaction within the sum-of-potentials (SOP) approxi-
4 mation, thereby effectively disregarding, at least initially, the role of 3B forces and of other
5 corrections: this is usually a realistic approximation whenever very diffuse states are ex-
6 pected to characterize most of the system bound states; (iii) one can then select the partner
7 masses either as the most common isotopic mixture or as a specific isotopic value; (iv) one
8 finally generates the rotationless ($J=0$) vibrational spectroscopy of the three-particle system
9 and of the component 2B pairwise species. Once the above procedure has generated satis-
10 factory data, one can then carry our further studies by carefully varying the overall potential
11 strength in order to observe the possible appearance of Efimov states for the overall complex
12 and the induced modifications of the initial vibrational structures [9–11].

13
14
15
16
17
18
19
20
21
22
23
24
25
26
27
28
29
30
31
32
33
34
35
36
37
38
39
40
41
42
43
44
45
46
47
48
49
50
51
52
53
54
55
56
57
58
59
60
The object of the present study is therefore directed at the analysis of the steps of the
above procedure in the case of three different partners bound by very weakly forces as H,
He and Ne, where we intend to further probe the consequences of going beyond the SOP
approximation by considering 3B contributions. We shall analyse the final structures by also
varying the isotopic masses of the atomic partners in order to gauge the "tuning" features of
the particle masses in terms of potential modifications. Most of all, we intend to show that
the use of Distributed Gaussian Functions (DGF) for the generation of the three-particle
bound states can provide a numerically stable procedure for assessing both the isotopic
variations and the 3B corrections of the three-particle spectral structure. These findings
could therefore give us the necessary confidence on the numerical robustness of the method
for the search of possible Efimov features once the overall potential is modified [9, 10].

The paper is organized as follows: the next Section II briefly outlines the DGF variational
expansion. The latter method has been presented many times before [9–13] and therefore
only a short summary of its implementation will be given below, referring any interested
reader to our earlier publications. Section III describes the 2B potentials employed for the
two title systems and the 3B corrections which we have included, while Section IV presents
our results. The conclusions are drawn in section V.

Although, as far as we are aware, there are no vibrational spectra measurements available
for the title systems, we think that their special features as weakly bound complexes still
warrant a detailed study to provide us with some physically realistic benchmark data on the
vibrational structures which they are expected to have.

The choice of the present systems is also motivated by their being able to support either

one or only very few bound states with the existing potentials and therefore capable of possibly showing Efimov behavior when these potentials are modified. An initial assessment of such an analysis is also given in section IV.

II. THE DGF METHOD

When one assumes a pairwise interaction as a description of the total potential energy surface (PES) for the ABC systems we are discussing here, then the approximation employed goes under the name of the sum-of-potentials (SOP) approximation, given as a simple addition of atom-atom potentials, each depending on a single bond distance R_i ,

$$V_{\text{tot}}(R_1, R_2, R_3) \simeq [V_1(R_1) + V_2(R_2) + V_3(R_3)]. \quad (1)$$

The corresponding Hamiltonian, and the corresponding configuration space volume element, can be expressed in atom-atom coordinates (R_1, R_2, R_3) using the masses of the three atomic partners (m_1, m_2, m_3) . The specific expressions have been given recently by us [14] and will not be repeated here again.

Within the present approach, the total wave function for the k -th vibrational bound state is expanded in terms of basis functions which explicitly depend on (R_1, R_2, R_3)

$$\Phi_k(R_1, R_2, R_3) = \sum_j a_j^{(k)} \phi_j(R_1, R_2, R_3). \quad (2)$$

When the system contains no identical atomic partners one can write

$$\phi_j(R_1, R_2, R_3) = N_{lmn}^{-1/2} \varphi_l(R_1) \varphi_m(R_2) \varphi_n(R_3). \quad (3)$$

Here, j denotes a collective index such as $j=(l; m; n)$. The corresponding normalization constants, N_{lmn} , are

$$N_{lmn} = s_{ll} s_{mm} s_{nn}, \quad (4)$$

which are expressed in terms of the overlap integrals

$$s_{pq} = \langle \varphi_p | \varphi_q \rangle. \quad (5)$$

As suggested by Hamilton and Light [15], each one-dimensional function φ_p is chosen to be a DGF centered at the R_p position

$$\varphi_p(R_i) = \sqrt{\frac{2A_p}{\pi}} e^{-A_p(R_i - R_p)^2}. \quad (6)$$

The coefficient A_p is defined in terms of the distance between the centers of φ_{p-1} and φ_{p+1}

$$A_p = \frac{4\beta}{(R_{p+1} - R_{p-1})^2}, \quad (7)$$

with the exception of the first and last DGFs whose A_p are given by $A_1 = \beta/(R_2 - R_1)^2$ (R_1 and R_2 being the centers of the first and second DGF) and, if we consider M DGFs, $A_M = \beta/(R_M - R_{M-1})^2$, where β is a dimensionless parameter close to one: we chose $\beta=1.05$.

In order to fulfill the triangle requirement between interatomic distances, the product $\varphi_l \varphi_m \varphi_n$ will belong to the basis if the DGF centers, R_i , satisfy

$$|R_l - R_m| < R_n < R_l + R_m. \quad (8)$$

Note that Eq.(8) corresponds to a more restrictive inequality condition, instead of the classical triangular inequality requirement (TIR) ($|R_l - R_m| \leq R_n \leq R_l + R_m$), to avoid unphysical behavior of the total wave functions at the triangle's boundaries, a point we have discussed at length in our recent work [14].

The eigenvalues of the DGF Hamiltonian are calculated by means of a standard iterative projection eigensolver [16], which enables us to extend the earlier size of the DGF expansion from about 60,000 basis functions to a fully converged size of about 630,000 functions.

Each ϕ_j basis function identifies a set of three interatomic distances which is in turn related to a triangle configuration and, therefore, quantities such as the area (from the *Heron formula*), cosine values of any angle of a triangle (from the *cosine theorem*) or the diameter of the circumscribed circumference (from the *sine theorem*) can be evaluated to obtain spatial nuclear distributions and the most probable geometries of the triatomic system at hand [14].

From the normalization condition of the total wave function something like a weight $P_j^{(k)}$ can be extracted for each j -configuration

$$1 = \langle \Phi_k | \Phi_k \rangle = \sum_j a_j^{(k)} \langle \Phi_k | \phi_j \rangle = \sum_j P_j^{(k)}. \quad (9)$$

Although the sum of the quantities $P_j^{(k)}$ is effectively equal to one, their character is not necessarily positive and therefore prevents them to be considered proper statistical weights. Despite this drawback, however, we have already shown that they enable us to estimate the number and types (linear, isosceles, equilateral and scalene) of nuclear triangular configurations which are present in the triatomic system [17, 18] due to the quasi diagonal form of the overlap matrix whose elements are defined by Eq.(5).

In order to classify them as such, a certain minimum variation on the side lengths of the triangles has to be accepted: obviously, the minimum step-size Δ of the R_i -grid is the natural choice for the measure of this degree of "floppiness". One could, of course, make different choices as we have discussed in our earlier work [17] since the selection of rigid structures is an arbitrary simplification with only pictorial value. As an example, the basis function ϕ_j will be classified as "collinear" if the centers of its three Gaussian functions satisfy the relation $|R_i + R_j - R_k| < \Delta$ in one of the possible permutations. Analogously, if two of the three centers' values differ by no more than Δ and the third center's value is either larger (flat isosceles) or smaller (tall isosceles) than the other two, the corresponding ϕ_j will belong to the isosceles family.

We can also define the weight of each type of triangular family for each bound state k by summing the PWs $P_j^{(k)}$ associated to each element of the family:

$$W_{\text{type}}^{(k)} = \sum_{j=1}^{N_{\text{type}}} P_j^{(k)}, \quad k \in \text{type}. \quad (10)$$

Finally, the moments of a given magnitude x for the $|k\rangle$ bound state can be calculated resorting to the *mean value theorem*:

$$\langle x^n \rangle_k = \sum_j a_j^{(k)} \langle \Phi_k | x^n | \phi_j \rangle \approx \sum_j P_j^{(k)} x_j^n \quad (11)$$

where we have assumed that the magnitude x , depending on the three bond coordinates, has been replaced by a mean value corresponding to the triangular configuration described by the ϕ_j -function.

In order to quantify, for a given basis set, the relevance of the spatial subdomain where the total wave function for each vibrational bound state is unphysically non-zero, we introduce the badness operator \mathcal{W} , which "measures" the deviation from the TIR condition of Eq.(8) [14]

$$\mathcal{W}(R_1, R_2, R_3) = \begin{cases} 0, & |R_1 - R_2| \leq R_3 \leq R_1 + R_2 \text{ holds} \\ 1, & \text{otherwise.} \end{cases} \quad (12)$$

This operator can be easily represented in terms of DGFs as:

$$\begin{aligned} \mathcal{I}(ll', mm', nn') &= \langle \varphi_l(R_1) \varphi_m(R_2) \varphi_n(R_3) | \mathcal{W} | \varphi_{l'}(R_1) \varphi_{m'}(R_2) \varphi_{n'}(R_3) \rangle \\ &= \frac{1}{2} s_{nn'} \int_0^\infty \int_0^\infty dR_1 dR_2 \varphi_l(R_1) \varphi_{l'}(R_1) \varphi_m(R_2) \varphi_{m'}(R_2) \\ &\quad \cdot \left\{ 2 + \operatorname{erf} \left[\sqrt{A_{nn'}} (|R_1 - R_2| - R_{nn'}^\dagger) \right] - \operatorname{erf} \left[\sqrt{A_{nn'}} (R_1 + R_2 - R_{nn'}^\dagger) \right] \right\} \end{aligned} \quad (13)$$

where $\operatorname{erf}(x)$ is the error function while $A_{nn'}$ and $R_{nn'}^\dagger$ are the width and center respectively of the product of two Gaussian functions $\varphi_n \varphi_{n'}$. The whole point here is that we evaluate the integrals $\langle \phi_j | x^n | \phi_{j'} \rangle$ as the mean values of the x^n operator over the configuration $\phi_j \phi_{j'} = \phi_{jj'}^\dagger$

$$\langle \phi_{j=l,m,n} | x^n | \phi_{j'=l',m',n'} \rangle \cong x^n (R_{ll'}^\dagger, R_{mm'}^\dagger, R_{nn'}^\dagger). \quad (14)$$

Hence

$$\begin{aligned} \mathcal{I}(ll', mm', nn') &\approx \frac{1}{2} s_{ll'} s_{mm'} s_{nn'} \left\{ 2 + \operatorname{erf} \left[\sqrt{A_{nn'}} \left(|R_{ll'}^\dagger - R_{mm'}^\dagger| - R_{nn'}^\dagger \right) \right] \right. \\ &\quad \left. - \operatorname{erf} \left[\sqrt{A_{nn'}} \left(R_{ll'}^\dagger + R_{mm'}^\dagger - R_{nn'}^\dagger \right) \right] \right\}. \end{aligned} \quad (15)$$

This expression, together with the coefficients of the total wave function Φ_k in the chosen basis set, $\{\phi_j(R_1, R_2, R_3), j = (l, m, n)\}$, is used to estimate through the average value $\langle \mathcal{W} \rangle$ how much the norm of the wave function differs from the “reduced” norm, which we call the TIR-norm, integrated only in the domain where the TIR is satisfied.

In order to obtain a well behaving wave function which minimizes the “badness” indicator, high quality basis sets are obtained only with having Gaussian functions distributed along the three distances with the same step Δ (or multiple of Δ). The location of the N DGF centers are defined according to the formula introduced in [18]

$$R_i = n \cdot \Delta + i \cdot \Delta, \quad i = 0, 1, 2, \dots, N-1, \quad (16)$$

where the value of n provides the correct multiple of Δ which radially locates the position of the first DGF.

As thoroughly discussed in Ref.[18] the previous formula provides, for a given step Δ , the gaussian basis set which minimizes the extension of the spatial domain where the TIR is

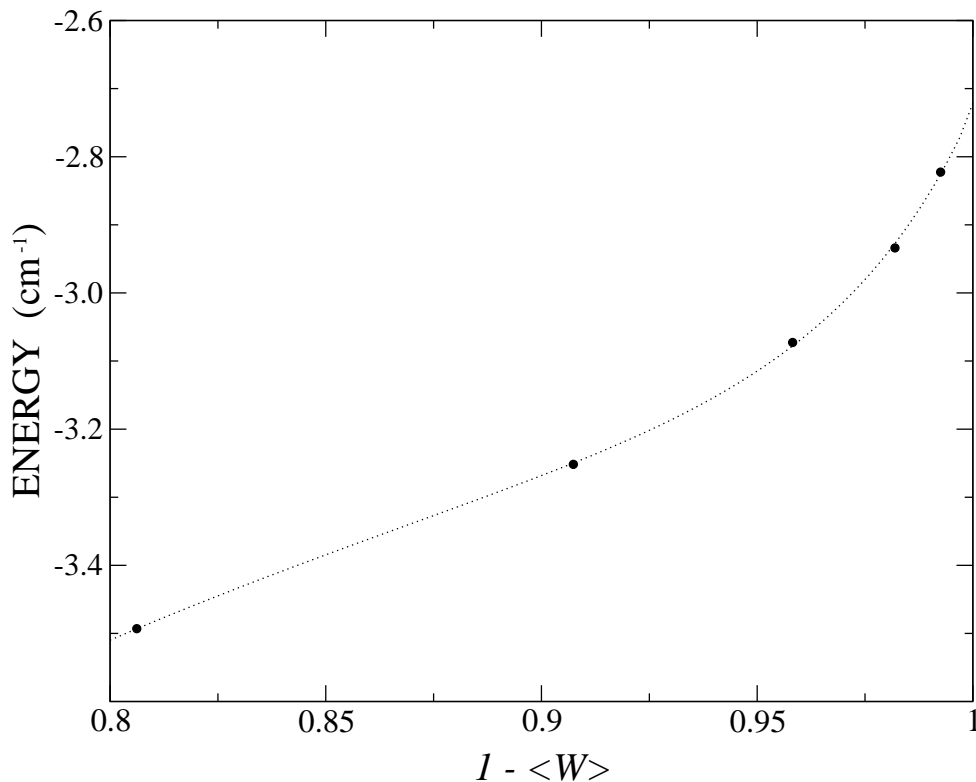


FIG. 1: Energy limiting value for the HeNeH system as a function of $(1 - \langle W \rangle)$. See text for details.

not satisfied. However, though negligible, the badness indicator is not zero even for the best basis set. By varying the initial location of the first DGF we can modify the relevant badness and, by plotting the ensuing energy value as a function of the “goodness” $(1 - \langle W \rangle)$, we can extrapolate up to zero badness in order to extract the best bound state energy. Typically, we shift the location of the DGF centers according to the following formula:

$$R_i = \left(n + \frac{x}{10}\right) \cdot \Delta + i \cdot \Delta, \quad i = 0, 1, 2, \dots, N - 1; x = 0, 1, \dots, 10 \quad (17)$$

Finally, we repeat the above procedure by choosing a smaller Δ and, by plotting the zero badness energy values obtained for each chosen Δ , we can in turn extrapolate at the exact δ -Dirac limit ($\Delta = 0$).

The results of Fig.1 relate to the lowest bound state of the HeNeH system: we see that the energy limiting value, i.e. -2.7165 cm^{-1} , essentially coincides with the one from Ref.[19], i.e. -2.7122 cm^{-1} .

The previous expression yields a well-behaving basis set in the sense of making the devia-

TABLE I: Characteristic parameters for the pairwise potentials employed in this work. Distances in a_0 and energies in cm^{-1} . See main text for details.

	He-Ne	He-H	Ne-H
D_e	14.47	4.70	16.46
r_{eq}	5.76	6.77	6.13
r_0	5.16	5.99	5.37
E_b	2.386	–	0.456
	He-Ne	He-H ⁻	Ne-H ⁻
D_e	14.47	3.23	26.36
r_{eq}	5.76	12.81	8.70
r_0	5.16	10.57	7.11
E_b	2.386	0.397	12.519 ($\nu=0$)
	–	–	1.082 ($\nu=1$)

tion from the TIR negligible. Once the three 1D grids have been chosen, the basis functions $\phi_j(R_1, R_2, R_3)$ are built as normalized products of three DGFs, each one defined along a different atom-atom distance and whose centers verify the TIR of Eq.(8).

III. MODELLING THE FULL PES

A. Pairwise Potentials

The three interactions employed at this level of approximation were already described in detail by Ref.[14], so we will summarize them only briefly in the following paragraphs.

The rare-gas (Rg) potentials were taken to be given by the multiparameter form proposed by Tang and Toennies [20] while the hydrogen interactions with He and Ne atoms were taken from Ref.[21]. The interactions of the H⁻ with the two Rg atoms were those employed in our earlier work [13, 22] and had been calculated with highly correlated wavefunctions in Ref.[23].

The data collected in Table I summarize the specific features of the pairwise potentials, providing the values of the radial location of the potential minima (r_{eq}) and the depth of

the corresponding attractive wells (D_e). The radial values for the onset of the potentials' repulsive walls (r_0) are also reported in order to give us an idea about the size of their corresponding repulsive cores. The 2B binding energies (E_b) are also listed. The HeNe system is the most strongly bound subsystem among the pairwise potentials for neutral partners, of which the HeH pair is not bound [14]. Among the anionic pairs the NeH^- is the most strongly bound with two bound states while the anionic He- H^- pair only exhibits one bound state around 0.4 cm^{-1} [14].

The extension of the SOP approach to the three-particle systems has been discussed before and will not be repeated here [14]. In Table II, however, we report the specific angular values and the percentage weights for the "collinear" types of structures obtained in that study for the $k=0$ state of HeNeH^- , together with its average angles. When we compare such values with their average counterpart we can see both the "near-linear" features and the meaning of our classification in terms of triangular families. The chosen size of "floppiness" parameter, taken equal to Δ (see previous section) in the present study, allows for the near-collinear scalene configurations to be able to be counted in the collinear family and makes the classical representation in terms of rigid structures still usable for the description of a quantum, floppy system.

B. The 3B Corrections

For neutral partners the most important correction to the simpler SOP model for the full PES is the one associated with the triple-induced dipole forces among the three partners

TABLE II: Computed angular averages and percentage weights for the three allowed collinear structures (identified by the atom in the middle of the arrangement) and for the ground state $k=0$ of the anionic complex. All angular data are in degrees.

	$\theta_{\text{Ne}-\widehat{\text{He}}-\text{H}^-}$	$\theta_{\text{He}-\widehat{\text{Ne}}-\text{H}^-}$	$\theta_{\text{He}-\widehat{\text{H}^-}-\text{Ne}}$	W_{type}^k (%)
Coll (He)	149.7	19.8	10.6	0 %
Coll (Ne)	18.0	149.3	13.0	59 %
Coll (H^-)	12.0	15.8	152.4	0 %
$\langle \theta \rangle_{k=0}$	34.7	123.1	24.3	

[24] and which we know to provide at long range the Axilrod-Teller (AT) contribution to the full interaction [25]. In our previous study on the Ar₃ system, however, we had found [12] that the AT corrections were not very significant and did not substantially modify its spectral structure. Since we are dealing here with much more weakly interacting partners (in the HeNeH three-atom complex, at least) we did not consider it necessary to test its effects on the single bound state of the neutral cluster [14].

On the other hand, the charged complex containing H⁻ presents an additional, stronger effect associated with the polarization of the neutral atomic partners due to the dipolar interaction induced by the charged component H⁻: the induced dipoles could in turn interact with each other, thereby modifying the overall features of the full PES. The atomic polarizabilities of the He atom (1.38 a₀³) and of the Ne atom (2.669 a₀³) are taken from [26] and the effects of the dipole-dipole interaction can be written down as [27]

$$V_{3B} = -\frac{\mu_{\text{He}}\mu_{\text{Ne}}}{R_3^3}(2 \cos \phi_1 \cos \phi_2 - \sin \phi_1 \sin \phi_2) \quad (18)$$

where R_3 is the He-Ne atomic distance and the ϕ 's are the angles which the two dipoles form with the connecting axis containing R_3 . The dipole values can in turn be extracted from the relevant atomic polarizabilities at the dipolar level

$$\mu_{\text{He}} = \frac{\alpha_1}{R_2^2}; \quad \mu_{\text{Ne}} = \frac{\alpha_2}{R_1^2} \quad (19)$$

which finally yields the following expression

$$V_{3B}(R_1, R_2, R_3) = -\alpha_1\alpha_2 \left(\frac{3}{4} \frac{R_1}{R_2^3 R_3^5} + \frac{3}{4} \frac{R_2}{R_1^3 R_3^5} - \frac{1}{4} \frac{1}{R_1^3 R_2^3 R_3} \right. \\ \left. - \frac{1}{2} \frac{1}{R_1 R_2^3 R_3^3} - \frac{3}{2} \frac{1}{R_1 R_2 R_3^5} - \frac{1}{2} \frac{1}{R_1^3 R_2 R_3^3} \right) \quad (20)$$

One can therefore modify the full PES by adding the 3B term

$$V_{\text{full}}(R_1, R_2, R_3) = V_{\text{NeH}^-}(R_1) + V_{\text{HeH}^-}(R_2) + V_{\text{HeNe}}(R_3) + V_{3B}(R_1, R_2, R_3) \quad (21)$$

The final potential can then be used within the full hamiltonian and employed within the variational expansion discussed in the previous Section.

Another possible approach, in order to establish more qualitatively the importance of the above correction to the SOP model, could be had by considering the V_{3B} as a perturbation.

This implies solving first the variational equation with the first three terms on the r.h.s. of Eq.(21)

$$H^{(0)}\Phi_k^{(0)} = E_k^{(0)}\Phi_k^{(0)} \quad (22)$$

then constructing the perturbation matrix element with the potential of Eq.(20)

$$V_{3B}^{(k)} = \langle \Phi_k^{(0)} | V_{3B} | \Phi_k^{(0)} \rangle \quad (23)$$

through which we finally obtain the energy levels corrected to first order as

$$E_k = E_k^{(0)} + \sum_j V_{3Bj}^{(k)} P_j^{(k)} \quad (24)$$

where the $V_{3Bj}^{(k)}$ refers now to the matrix elements of the potential of Eq.(20) over the variational basis set for the k th state

$$V_{3Bj}^{(k)} = \langle \varphi_j | V_{3B} | \varphi_j \rangle. \quad (25)$$

We therefore need to perform the variational calculations only once for the $H^{(0)}$ hamiltonian of Eq.(22) and then correct its eigenvalues via the matrix elements of Eq.(25) in Eq.(24). We shall compare below the outcomes from these two different approaches in order to establish the perturbative strength of the 3B correction terms for the anionic cluster, the one which should be the more likely to be affected by them.

IV. RESULTS AND DISCUSSION

A. The 3B energy effects

The details of the basis set expansion and of the badness parameters obtained within the SOP approximation have been extensively given by Ref.[14] and therefore will not be repeated here. To summarize the findings for the HeNeH⁻ system, we report in the 2nd column of Table III the final, total energies obtained for the three rotationless states of that system computed via the SOP modeling of the full PES, as discussed in the previous Section.

We then obtained the variational results using the full PES of Eq.(21), generating the dipole-dipole terms with the polarisability values of Ref.[26].

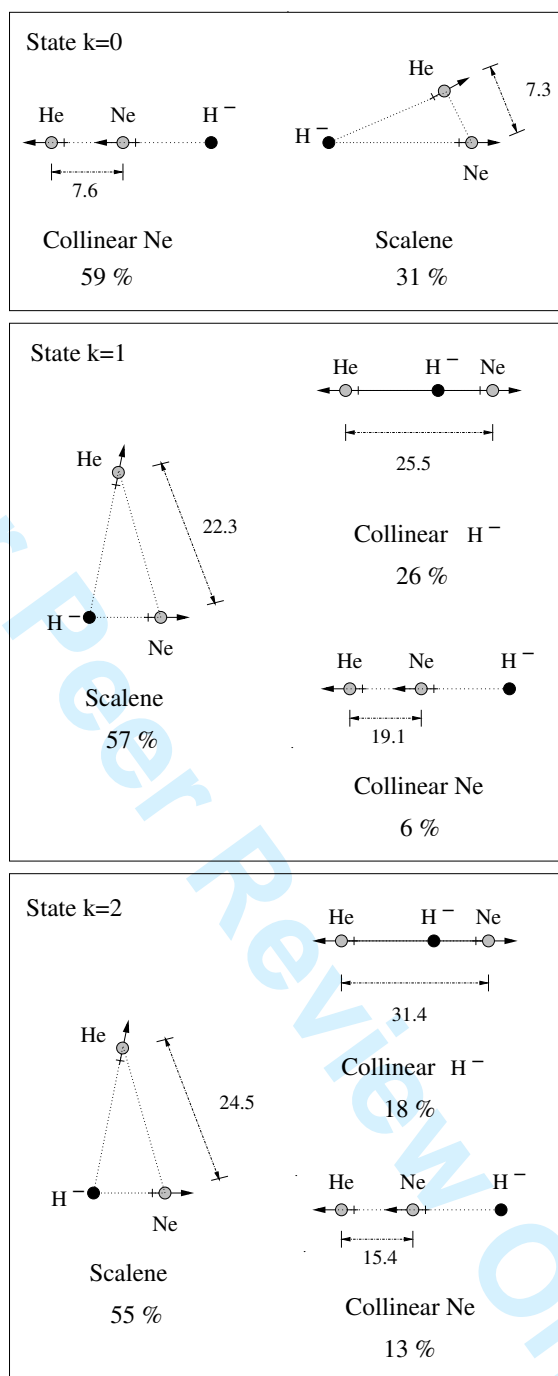


FIG. 2: Computed percentage weights for the dominant geometries of HeNeH^- , using the full PES of Eq.(21) within the variational treatment, for the three bound states of the system. Average distances in a_0 . See main text for further details.

TABLE III: Computed energy values in cm^{-1} for the $J=0$ states of the HeNeH^- complex. See text for details.

$ k\rangle$	$E_{\text{SOP}}^{\text{tot}(k)}$	$E_{\text{full}}^{\text{tot}(k)}$	$BE_{\text{SOP}}^{(k)}$	$\Delta E_{\text{full}}^{(k)}$	$\%V_{3B}^{(k)}$	$E_{\text{pert}}^{\text{tot}(k)}$	$V_{3B \text{ pert}}^{(k)}$
$k=0$	-16.2284	-16.2863	3.7095	$-5.79 \cdot 10^{-2}$	1.6	-16.2873	$-5.89 \cdot 10^{-2}$
$k=1$	-13.3461	-13.3433	0.8272	$+2.72 \cdot 10^{-3}$	0.3	-13.3426	$+3.50 \cdot 10^{-3}$
$k=2$	-12.7592	-12.7612	0.2403	$-2.03 \cdot 10^{-3}$	0.8	-12.7616	$-2.43 \cdot 10^{-3}$

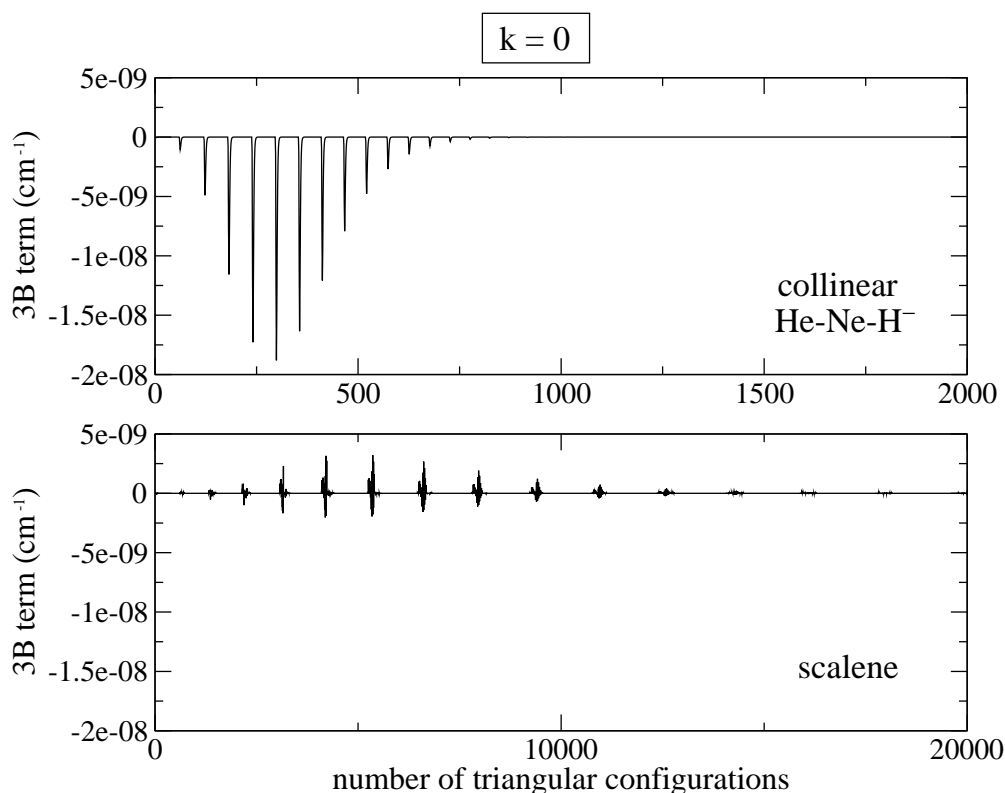


FIG. 3: Computed 3B contributions for each of the collinear (upper panel) and scalene (lower panel) present in the description of the $J=0$ ground vibrational state of HeNeH^- . The maximum values of the abscissae reflect the number of collinear and scalene basis functions. The quantities are the $V_{3Bj}^{(k)} \cdot P_j^{(k)}$ on the r.h.s. of Eq.(24). Only the range of non-negligible configurations is presented.

All the results reported by the various columns of Table III show the detailed findings of the present calculations. As mentioned above, the $E_{\text{SOP}}^{\text{tot}(k)}$ values refer to the variational

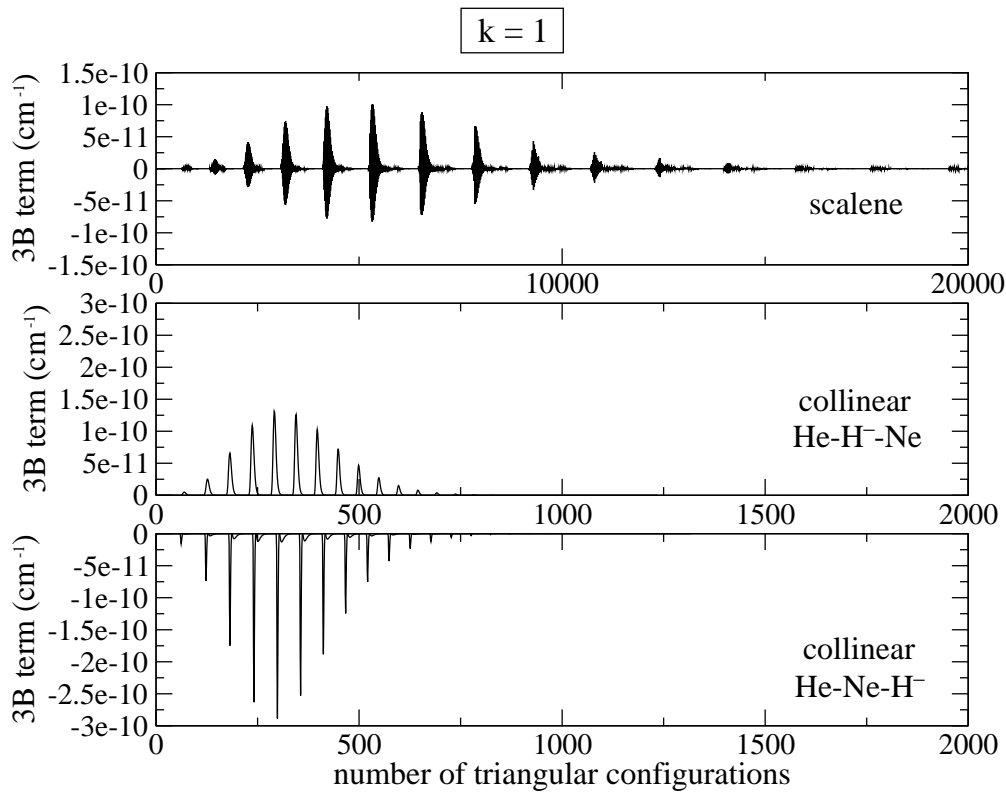


FIG. 4: Same as in figure 2 but for the three most important configurations of the $k = 1$ vibrational state.

calculations for the three states of the system using the simpler SOP form for the PES, while the total energies obtained with the full 3B potential, $E_{\text{full}}^{\text{tot}(k)}$, are given by the column of Table III labelled by the latter symbol. The quantity of column four, $BE_{\text{SOP}}^{(k)}$, gives the binding energies of each of the three levels with respect to dissociation. The $\Delta E_{\text{full}}^{(k)}$ data heading column five indicates the difference (3B correction) obtained from the previous two total energy values. We clearly see there that the modified basis set returns a 3B effect which is around 1 % at most of the actual binding energies ($BE_{\text{SOP}}^{(k)}$) reported in the 4th column. This is indicated by the values given by the $\% V_{3B}^{(k)}$ symbol that heads column 6. The corresponding values of total energy provided by the perturbative treatment, $E_{\text{pert}}^{\text{tot}(k)}$, are further listed by column 7 while in column 8 we report the 1st order correction $V_{3B \text{ pert}}^{(k)}$ given by the sum on the r. h. s. of Eq.(24). We see clearly that the changes of $E_{\text{SOP}}^{\text{tot}(k)}$ from column two are obtained just as accurately by the simpler perturbation treatment: they are close to the results given by the full variational approach shown by the $\Delta E_{\text{full}}^{(k)}$.

B. An Analysis of Configurations

On the basis of the dominant configurations which were obtained by the SOP variational results one can also analyse in more detail the specific effects of the 3B terms on the binding energies for each of the three states supported by the HeNeH^- potential for the $J=0$ case.

The pictorial schemes of figure 2 help us to understand such effects by first looking at the dominant configurations for the three bound states of the anionic system. The three panels of the figure report the percentage weights of the dominant structures and the "size" of them by giving the more relevant distances between atomic partners: the directions of the interacting dipoles induced by the H^- on the other two atomic partners are also explicitly indicated.

From the top panel, referring to the $|k=0\rangle$ state, we see that the dipole-dipole interaction is mainly attractive for the collinear structures while it is less so (and can even be repulsive) for the scalene structures. Such qualitative observation is borne out by the results of figure 2, where we show the specific correction matrix elements given by Eq.(25).

One immediately sees there that the corrections induced by the 3B term are invariably negative (stabilizing) in the case of the collinear structures while becoming smaller, but causing both stabilization and destabilization effects in the case of the scalene structures. Thus, we now understand why Table III shows a stabilized ground state of HeNeH^- when 3B effects are included.

The situation changes markedly when we now look at the $|k=1\rangle$ excited state of the same system, for which the individual 3B contributions to the binding energy are given in the three panels of figure 3 while the spatial orientations are sketched in the middle panel of figure 2.

The most important scalene structures show contributions which have both types of effects, i.e. either stabilizing or destabilizing. The two possible collinear structures have opposite effects depending on the relative location of the negative charge along the row of the three atoms. Hence, the net effect on the energy is now slightly destabilizing (see Table III). In both cases, however, the effects are much smaller than those found for the $|k=0\rangle$ level, as expected for a spatially more extended bound state.

The behavior of the 3B effects for the highest bound state of the system, the $|k=2\rangle$ level, is shown by the results of the three panels in figure 4, while the details of that state are

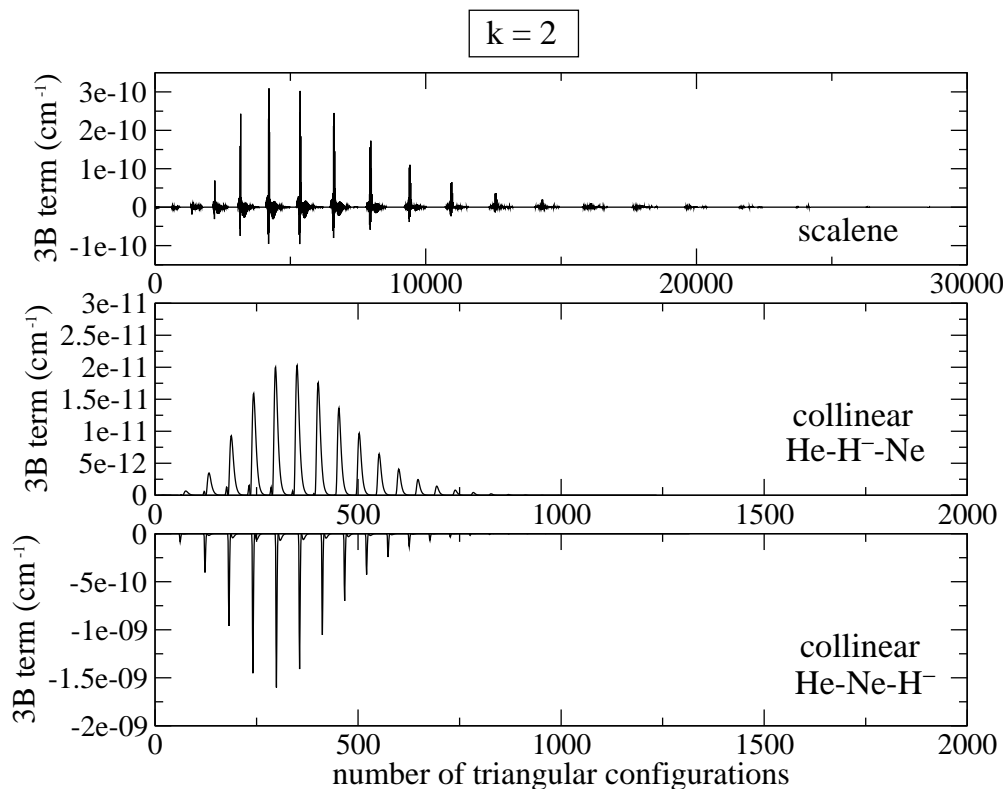


FIG. 5: Same as in figure 2 but for the dominant configurations of the $k = 2$ vibrational level of HeNeH^- .

given in the lowest panel of figure 2.

The calculations indicate again that the collinear and the scalene structures are the most likely to provide sizeable 3B corrections to the binding energy and that they will yield either stabilizing (negative) or destabilizing (positive) contributions depending, in the collinear case, on the location of the anionic partners and on the relative orientations of the induced dipoles. In this specific case, the final marked presence of the stabilizing collinear structures with the H^- on the outside of the complex (see figure 2), while those with H^- in the middle (and the scalene structures) have the induced dipoles which are too far apart from each other to counteract the latter effect, hence cause an overall energy lowering in the system.

One should again note at this point that the selection of a given triangular configuration to belong to a specific "shape" is somewhat arbitrary and depends, as discussed before, on the chosen minimum step size Δ of the radial grid. However, the overall quantitative data are independent of this choice while only the qualitative analysis in terms of "classical"

1
2
3 configurations would be slightly affected. We have discussed this point many times before
4 and refer the reader to our Ref.[17] for further details.
5
6
7

8 9 **C. The Spatial Representations**

10
11 In order to gain better insight over the actual spatial pictures of the vibrational states of
12 the present system, we report in figures 6 and 7 the particle 3D densities calculated for the
13 top two bound excited states separately integrated over each one of the radial coordinates.
14 Since the ground state is much more compact and rather featureless, we thought it more
15 interesting to focus this analysis on the two vibrationally excited states of the HeNeH^-
16 system.
17
18

19
20 One clearly sees from the picture in figure 6 the dominance of structures where the
21 H^- gets "attached" to the more polarizable Ne atom while the lighter He partner always
22 remains further away from the more compact anionic dimer: the two lower distributions, in
23 fact, indicate very marked differences in the actual values of the average distances of the
24 He partner from both Ne and H^- , while the distance between the latter two atoms is seen
25 to be, from both panels, always markedly smaller. Furthermore, the middle and top panels
26 show the nodal requirement for its orthogonality to the more compact ground state.
27
28

29
30 This feature is also apparent when we look at the same type of distributions for the next
31 vibrational level, the $|k=2\rangle$ level, reported by the three panels of figure 7.
32
33

34
35 The spatial extension of the density distributions has now increased and the nodal struc-
36 ture of the wave function is also more apparent since this final state needs to be orthogonal to
37 a more diffuse bound state (the $|k=1\rangle$ state) than was the case for the $|k=1\rangle$ wavefunction
38 depicted by figure 6. However, we still see that the NeH^- is the more compact "subsystem"
39 in the complex and that the three-atom aggregate can be described by a scalene structure
40 with an He atom further away with respect to the other two partners. Additionally, we see
41 clearly that the He is "sitting" equidistantly from the other two partners since its distances
42 from the Ne and H^- partners increase cogradiently with each other, while the opposite is
43 true when either of the other two distances is integrated out.
44
45
46
47
48
49
50
51
52
53
54
55
56
57
58
59
60

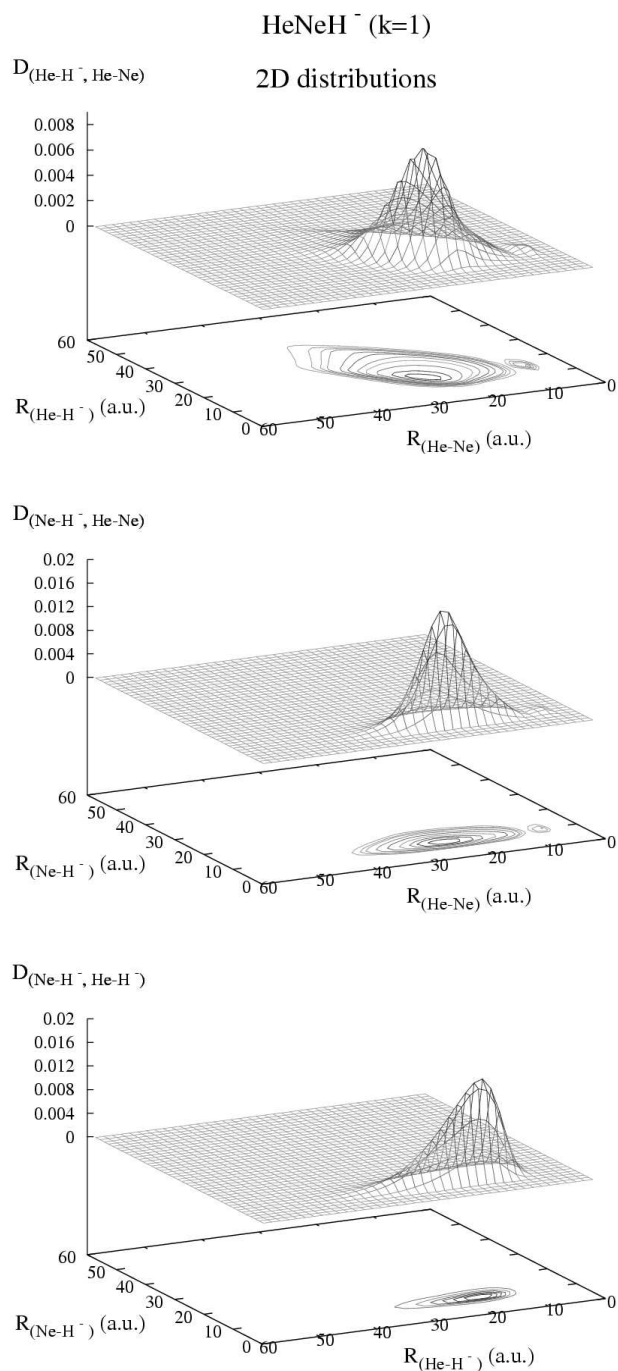


FIG. 6: Computed vibrational state ($k = 1$) 2D particle density distributions after integration over one of the radial variables. Top panel: after integration over R_{NeH^-} . Middle panel: integration over R_{HeH^-} . Bottom panel: integration over R_{NeHe} .

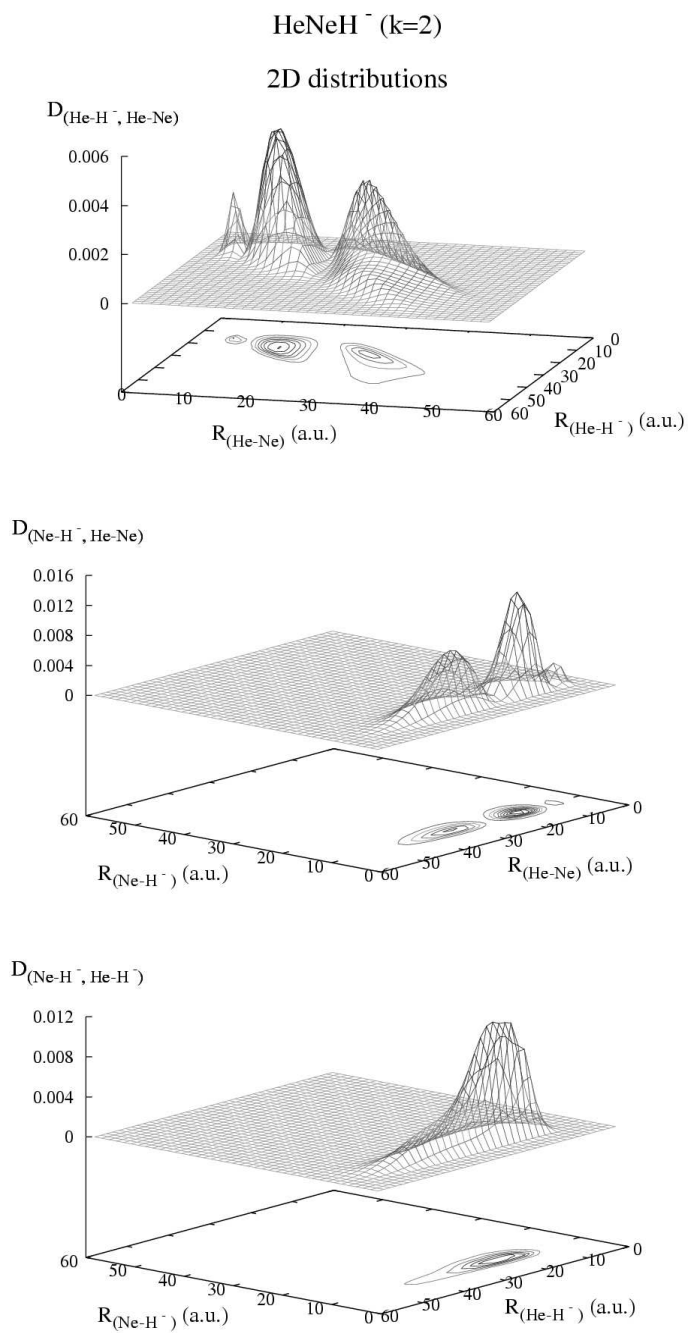


FIG. 7: Same as in figure 6 but for the next excited vibrational level in the HeNeH⁻ system. See text for details.

TABLE IV: Computed energy levels (cm^{-1}) for the isotopic variants of the diatomic partners.

ν	Ne-H ⁻	Ne- ² H ⁻	Ne- ³ H ⁻
0	-12.5189	-15.7478	-17.2776
1	-1.0820	-3.7871	-5.7696
2		-0.3164	-1.0908
3			-0.0504
	He-H ⁻	He- ² H ⁻	He- ³ H ⁻
0	-0.3968	-0.7622	-0.9512
	Ne-H	Ne- ² H	Ne- ³ H
0	-0.4562	-2.4411	-3.8380

D. The isotopic energy shifts

Another interesting source of “control” on the properties of these weakly bound systems could be had by examining the structural changes of the bound states when the mass of the lightest partner is modified. Due to the special nature of the hydrogen atom, in fact, the use of its isotopic variants, ²H and ³H, allows us to realistically (but smoothly) change the kinematics of the systems and therefore to computationally observe the consequences of such variants on the very few bound states of the complexes, a modification which could be in principle amenable to experimental detection.

The data reported by Table IV show the bound states for all the diatomic partners appearing in the two clusters studied in the present work. We shall focus the present analysis on the isotopic variations induced by the lightest partner, the H atom, since the latter is the one component which should provide the most interesting changes on the spectroscopy of the two title clusters. One sees, in fact, from the data of Table IV that the NeH⁻ shows the largest energy effects upon mass modification, as expected from the long-range nature of its interaction. The NeH⁻ molecule goes from having two bound states in the Ne¹H⁻ case to three for the deuterium partner, to four for the tritium partner. The other anionic molecule, on the other hand, simply shows a deepening of the single bound state location, as does the neutral diatomic NeH. The HeH system, however, does not acquire any bound state across

TABLE V: Energy levels of He, Ne,^(1,2,3) H and of He, Ne,^(1,2,3) H⁻ clusters (all in cm⁻¹).

k	He-Ne-H	He-Ne- ² H	He-Ne- ³ H
0	-2.7165	-4.8834	-6.3269
1		-2.5096	-3.8874
	He-Ne-H ⁻	He-Ne- ² H ⁻	He-Ne- ³ H ⁻
0	-16.2284	-19.6894	-21.3787
1	-13.3461	-16.7518	-18.2225
2	-12.7592	-16.3976	-18.1470
3			-17.5675
4			-17.3058

the whole isotopic variation from ¹H to ³H. It is also worth noting that the Ne^{2,3}H⁻ systems of Table IV indicate the appearance of very weakly bound (by less than 1 cm⁻¹) excited states.

The three-particle systems are analysed in Table V, where we report their total binding energies. In the case of the neutral complex we see that a 2nd bound state comes in after deuteration and that both bound states become more strongly bound after tritium replaces the D atom in the complex. The anionic cluster, on the other hand, shows a more marked effect of the mass changes on its bound levels, as expected from the long-range tail of the relevant potential. Thus, we find deeper bound states in the deuterated molecule and two additional states in the case of the tritium partner.

An analysis of the dominant classical configurations for the HeNe²H complex shows that, in contrast with the results obtained earlier for the HeNe¹H [14], the linear, or quasilinear, structures are dominant and always keep the D atom outside the HeNe partner: for the $|k=0\rangle$ state the picture is therefore that of a quasilinear triatomic with the D atom at one end of the structure. This effect could also be gleaned from the shape of the radial pair distributions obtained for the HeNeH upon deuteration. Their behavior is reported in the two panels of figure 8 where the new binding energies are also given.

We clearly see that the ground state has the D atom further away from the HeNe molecule and, as mentioned before, presents a nearly linear dominant configuration. The first excited

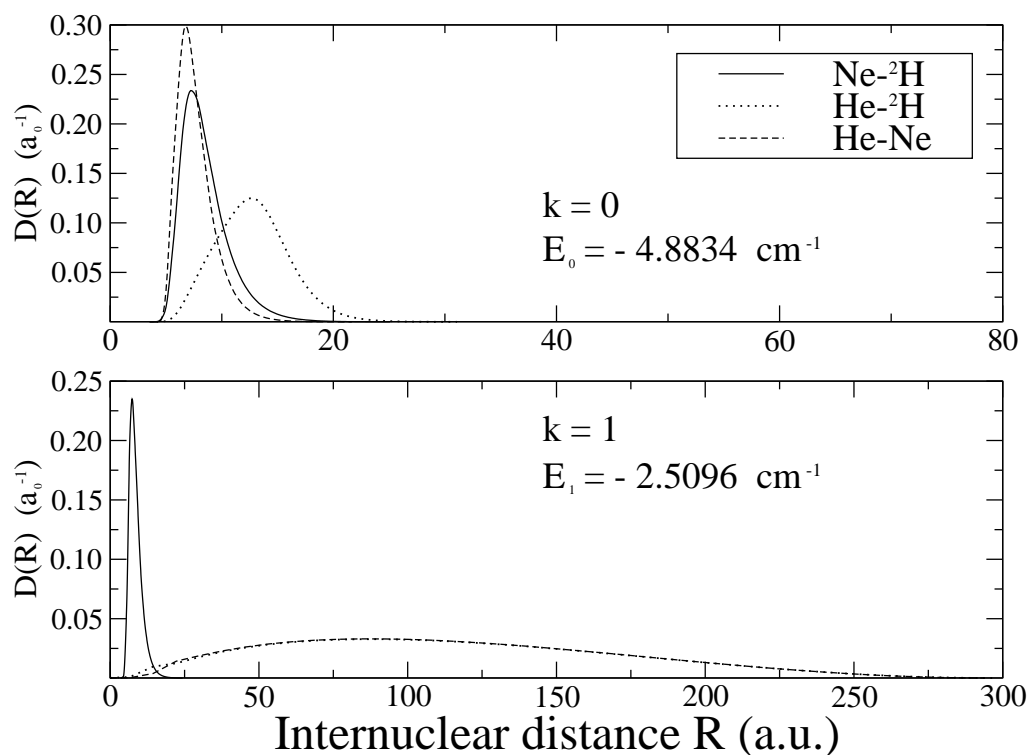


FIG. 8: Atom-atom radial density distributions (a_0^{-1}) computed in the deuterated complex Ne^2HHe . The symbols are explained within the figure.

state maintains a strongly collinear structure but now keeps the He atom further away from the NeD diatomic partner. The HeNeH complex, on the other hand, did not show any excited state but went directly into the H detachment process [14].

A pictorial view of this "threshold shifting" effect could be seen from the results reported by figure 9, where the sequential changes of fragmentation pattern are presented for the three isotopic variants of the HeNeH weakly bound complex.

As discussed more in detail in our previous work [14], the first fragmentation threshold appears for the hydrogen detachment, while the He detachment occurs at higher energies. As we perform the deuteration, however, we see that the appearance of another (excited) bound state causes the He atom to move further out and therefore the first dissociation now occurs with the loss of the He atom, leaving the D partner still bound to the Ne atom. The situation remains essentially unchanged, albeit more marked, when the T atom replaces the deuterium partner. It is interesting to note that the energies of both diatomic partners,

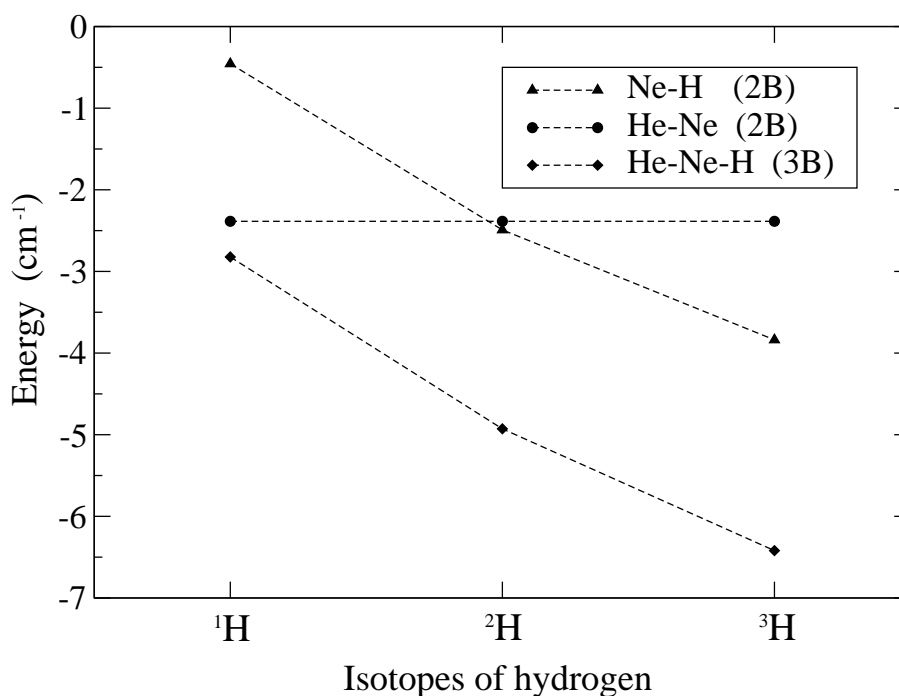


FIG. 9: Sequential presentation of the energy thresholds in the HeNeH complex as a function of the three isotopic variants containing ^1H (left panel), D (central panel) or T (right panel).

as expected, remain above the 3B energies along the whole sequence: hence, no Efimov scenario is expected, even for the isotopic variants, unless the potential strength were to be more drastically modified. Since the NeD binding energy becomes stronger upon deuteration than that of the HeNe complex, the latter subsystem dissociates first upon excitation of the three-particle cluster. This tendency is further reinforced when tritium replaces the D atom within the cluster.

Figure 10 finally summarizes schematically the changes of the energy structure of the HeNeHe system upon isotopic substitution.

E. Searching for Efimov states

It is well known that the possible existence of Efimov states is very sensitive to changes in the 2B interactions and therefore to the 2B binding energies [2, 10]. Hence, one of the

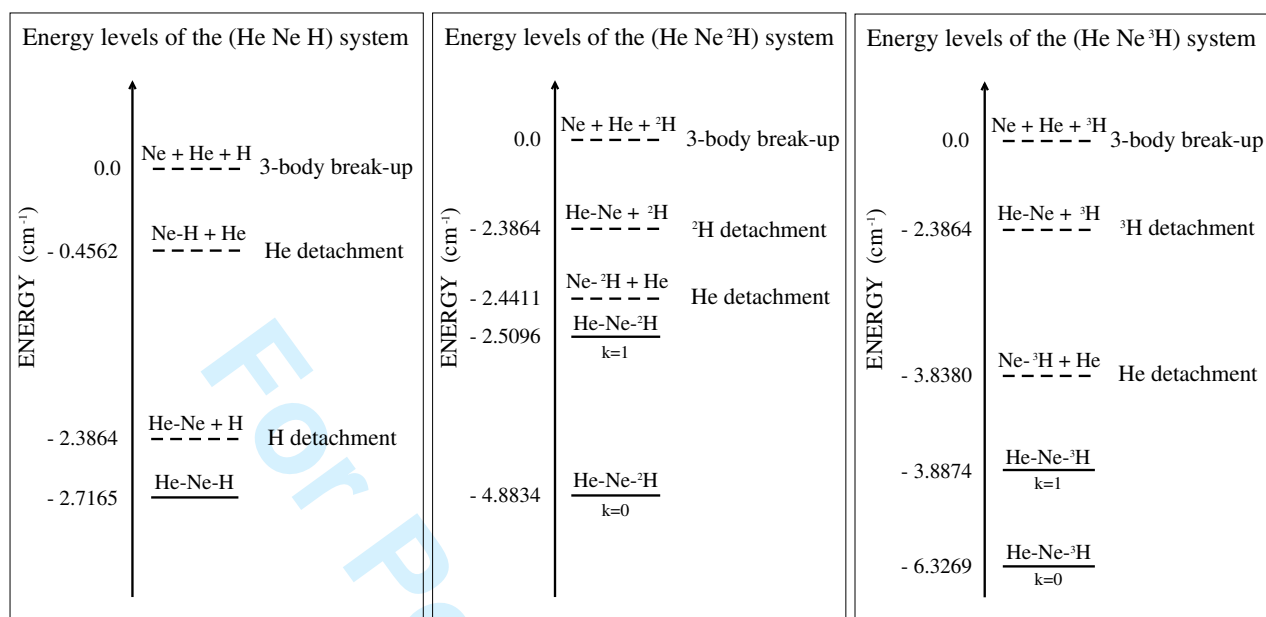


FIG. 10: Computed energy values of the lowest level in the HeNeH system as a function of the hydrogen isotopic present in the complex. The corresponding diatomic energy levels are also shown.

more common ways to characterize such states is to carry out an analysis of the discrete spectrum of the three-body system by varying the strength of the 2B interaction potential through a factor λ [10, 11]. For λ values < 1.0 it may be possible to detect the appearance of "halo" states of the 3B system when the corresponding 2B potentials have no bound states [2], while the Efimov states should appear for that range of increased λ values where they remain below the 2B bound state continuum threshold(s) and finally, as λ increases, are overrun by the threshold and the first excited state of the trimer above the 2B continuum threshold gives rise to a "ghost" state [28] or, more clearly, to a Feshbach resonance between the bound dimer and the "scattering" third atom of the complex [29]. In the present study we have looked at the λ dependence of the excited bound states of the HeNeH⁻ trimer and also of the only bound state of its neutral counterpart.

The idea was to see if, within a realistic range of variation of the values of λ , one could indeed label any of the excited states as having Efimov characteristics. Figures 11 and 12 report the λ changes for each of the systems and analyse the dependence of both the 2B bound states as a function of changing this parameter.

One clearly sees in figure 11 that the only bound state of the HeNeH system behaves

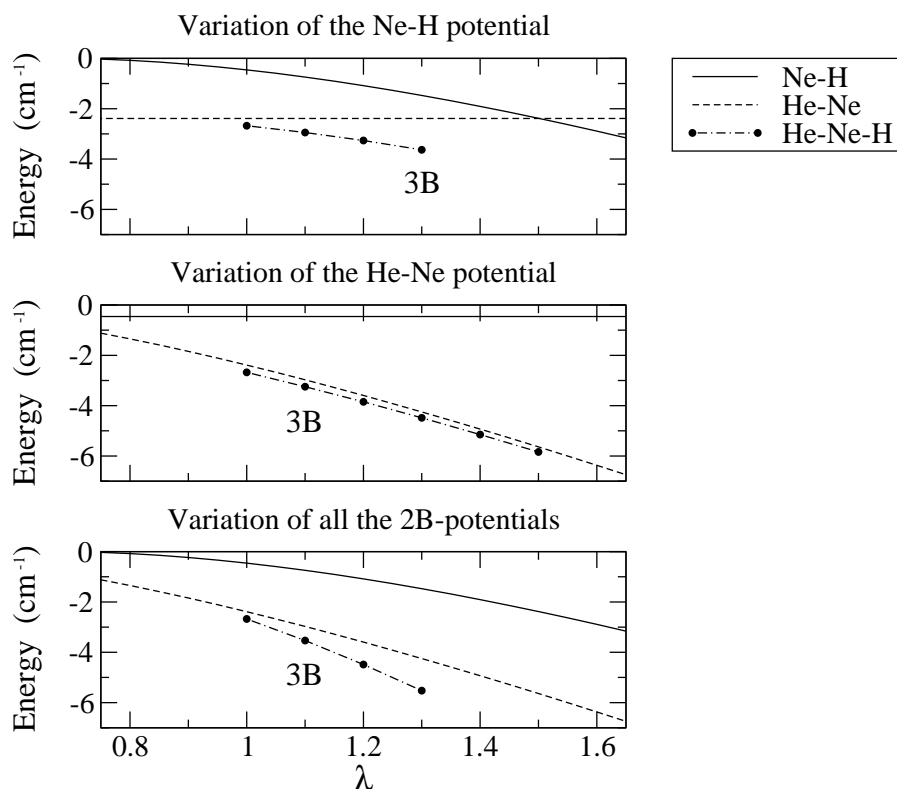


FIG. 11: Dependence of bound-state energies as function of the arbitrary parameter λ . The upper two panels report the 2B binding energy variations and the corresponding 3B values. The bottom panel shows the effect on the 3B binding energy as all 2B potentials are changed. The HeH interaction is not shown since it never supports bound states in chosen range of λ values.

as a conventional bound state in the sense that its binding energy increases as λ (potential strength) is increased and it does so faster than any of the component 2B binding energies. The data of figure 12 further indicate that none of the excited states of the anionic system acquires Efimov behaviour as λ increases for all relevant potentials and therefore they never generate "ghost" states for higher λ values (lower-right panel in figure). On the other hand, we see a very puzzling result when we vary only the strongest of the 2B potential, as done in the upper-left panel of the figure. We see there, in fact, that all three bound states show a λ value for which these states behave as Efimov states. Although the classical definition of the λ variation was introduced for three identical particles [2], it is interesting to see here that to strengthen only one of three different 2B potentials is creating the conditions for the appearance of an Efimov state.

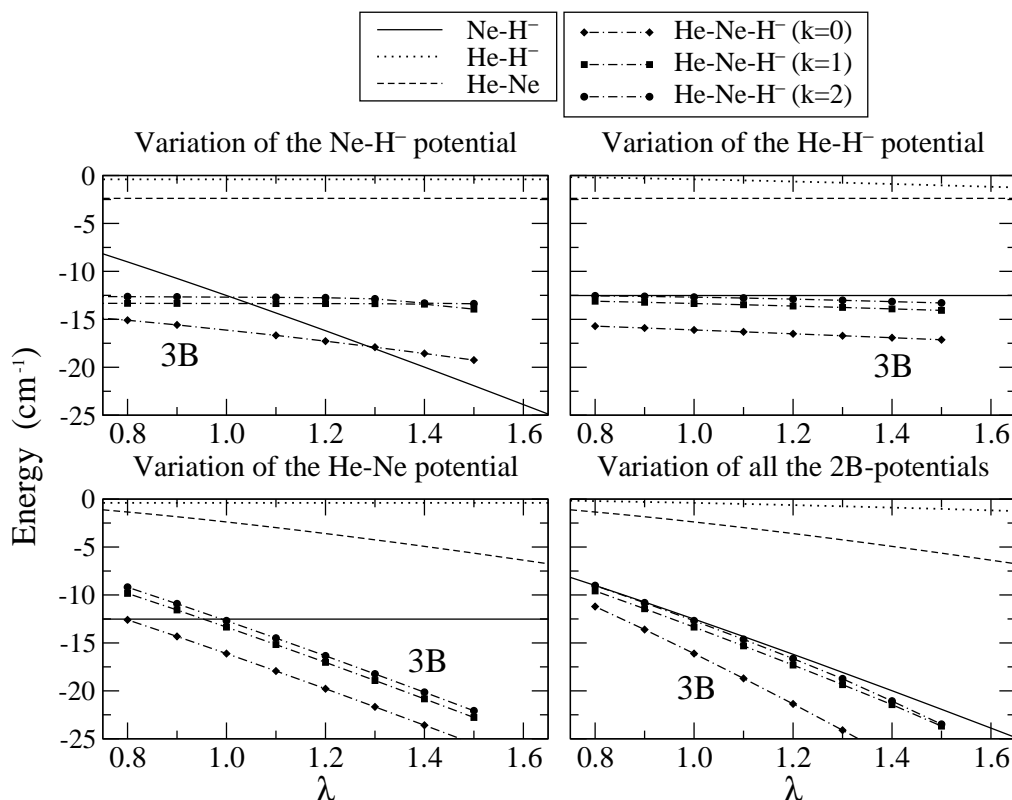


FIG. 12: Same as in figure 11 but for the anionic system. Three of the panels show the effect on the 3B energy as each of the 2B potentials is varied, while the fourth panel (bottom right) shows 3B energy variation as all the three 2B potentials are varied.

V. PRESENT CONCLUSIONS

This study of weakly bound complexes has employed a variational expansion over Gaussian functions, the DGF method used by us to study several other similar systems [9–12, 14, 18], in order to analyse specific effects on the bound-state structures of the two title systems: the contribution of dipole-dipole interaction in a charged environment (the HeNeH⁻ cluster) and the effects of isotopic and potential strength variations for both systems.

The addition of 3B forces has been analysed in two different ways, which were found to be very largely equivalent, and their consequences on the structural shape of the bound states, and on their binding strengths, has been discussed in detail. Our study is able to assign to specific spatial configurations the stabilizing or destabilizing role after 3B forces are included, thanks to the possibility offered by the DGF method to extract configurational weights from

1
2
3 the variational calculations. On the whole, however, our study finds the 3B forces to play a
4 rather minor role in determining the location of the bound states and their dominant spatial
5 shapes and that, in any event, our method can easily evaluate their importance.
6
7

8
9 Since this was found to be the case for the anionic complex, we could conclude that the
10 even more weakly bound neutral system can be realistically treated via the SOP description
11 of its full interaction.
12

13
14 The analysis of the isotopic variants has been focussed on the H atom and its effects have
15 been seen on both systems. The anionic complex increases its rotationless series of bound
16 states from 3 to 5 upon tritium replacement while the neutral system adds one extra bound
17 state when HeNeD and HeNeT are analysed.
18
19

20
21 The structural changes of the more weakly bound HeNeH complex have been looked at
22 in more detail and indicate that the 2B components, upon changing their binding energies,
23 cause a "threshold shifting" in the sense that He detachment becomes the lowest dissociation
24 threshold in the deuterated system, the effect becoming even more visible when T replaces
25 D in the three-atoms complex.
26
27
28

29
30 We have also employed the SOP scheme to search for Efimov states in both trimers by
31 arbitrarily varying the potentials' strength around their initial values ($\lambda = 1$) and found that
32 none of the bound states acquires Efimov character by using this conventional parametric
33 sensitivity test. However, the HeNeH⁻ system does show Efimov behaviour when the λ
34 variation only applies to one of the 2B potentials.
35
36
37

38
39 The present conclusion for the neutral trimer system is in agreement with the findings
40 of a recent study [29] where it was shown that short-range potentials as those existing for
41 ⁴He trimers cannot support Efimov states, a fact indicated already by experiments [30] on
42 that system. In conclusion, the use of the present variational approach, and its capability of
43 describing floppy systems as the result of generating several "classical" structures describing
44 the nuclear positions, has been shown capable of telling us, at the nanoscopic level, the
45 consequences of adding 3B forces to the simpler SOP modelling (very minor consequences)
46 and also capable of illustrating in detail the changes brought by isotopic substitutions on
47 very delocalized molecular clusters. Considering the current search for Efimov scenarios in
48 three-atom complexes [28], and for ways of externally modifying interaction forces in order
49 to reach a likely Efimov regime, the present study explicitly allows us to explore the physical
50 consequences of selectively changing the strength of the 2B interactions in floppy three-atom
51
52
53
54
55
56
57
58
59
60

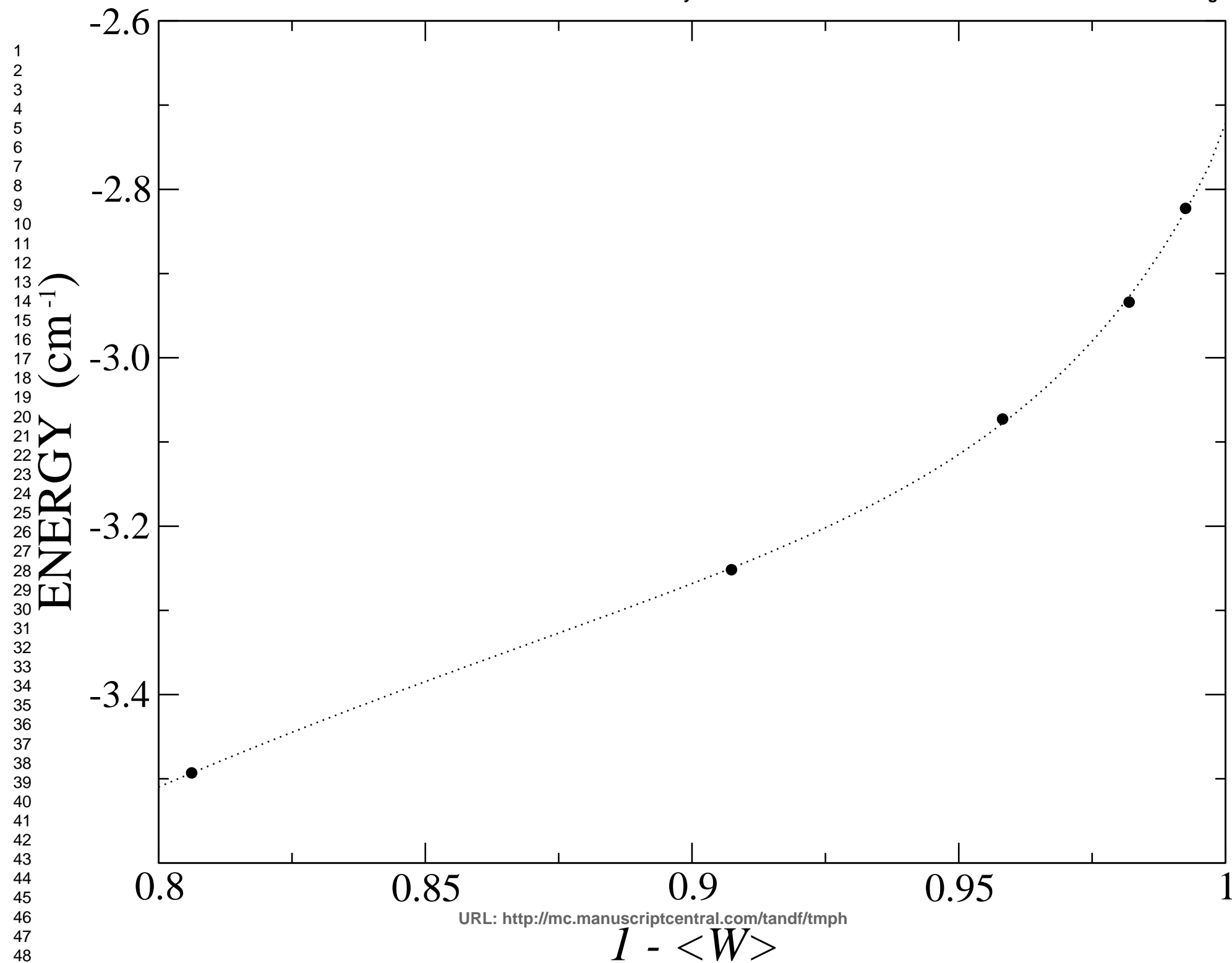
1
2
3 complexes. It also gives evidence about the robustness of the DGF approach for providing a
4 realistic evaluation of weakly bound states in special VdW systems and about its sensitivity
5 to small changes in the employed potential functions. Reassured by the present results, we
6 are currently testing the response of the present method for the analysis of possible Efimov
7 states in other systems (e.g. Cs_3) currently employed in experimental searches of such states
8 [31].
9
10
11
12
13
14

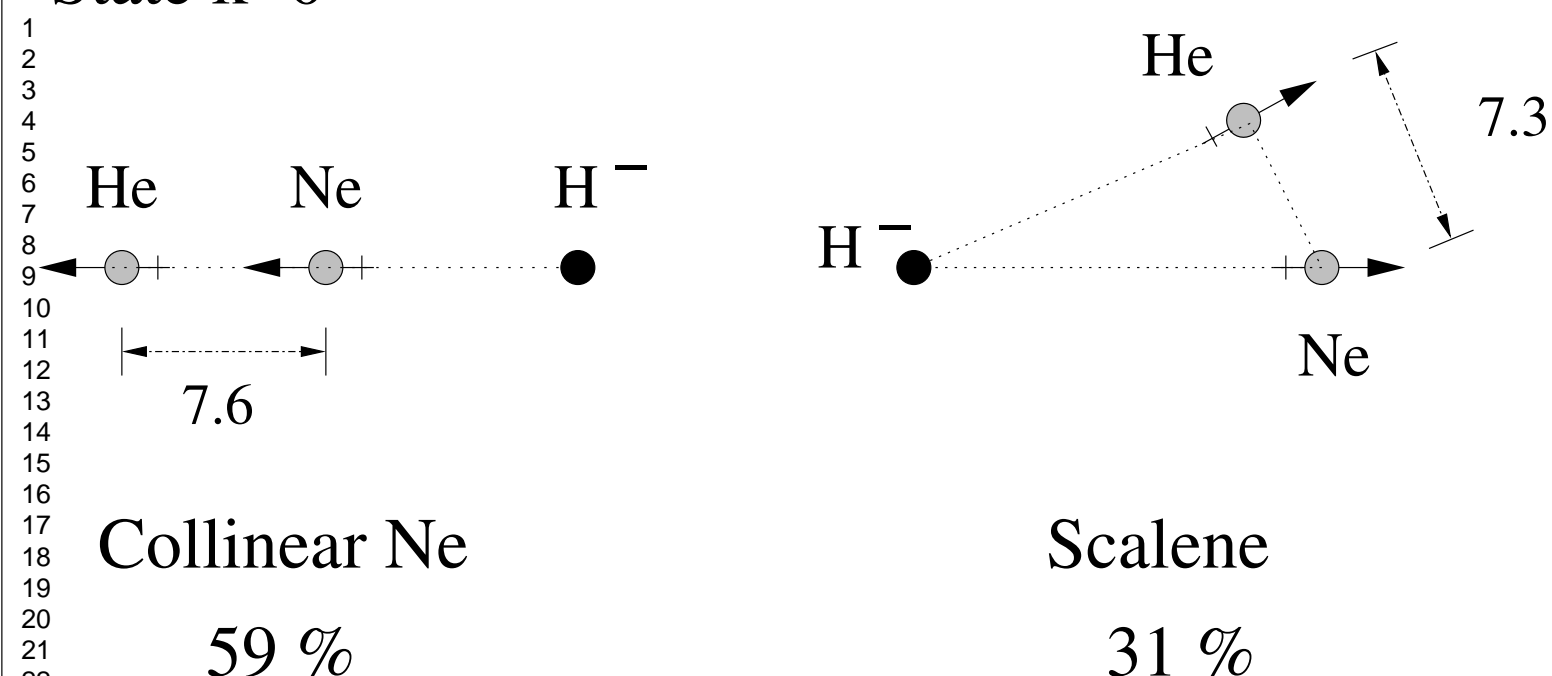
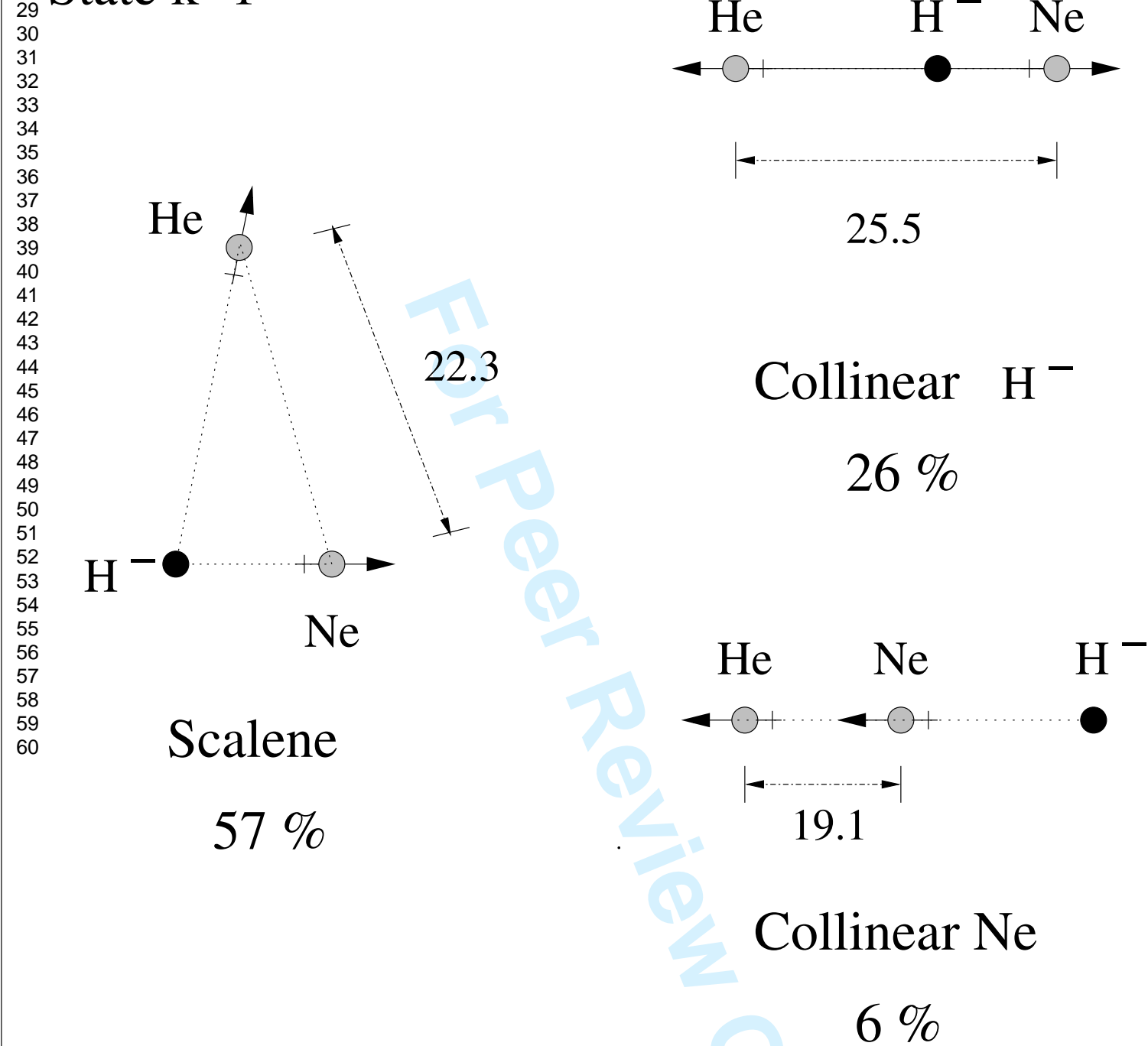
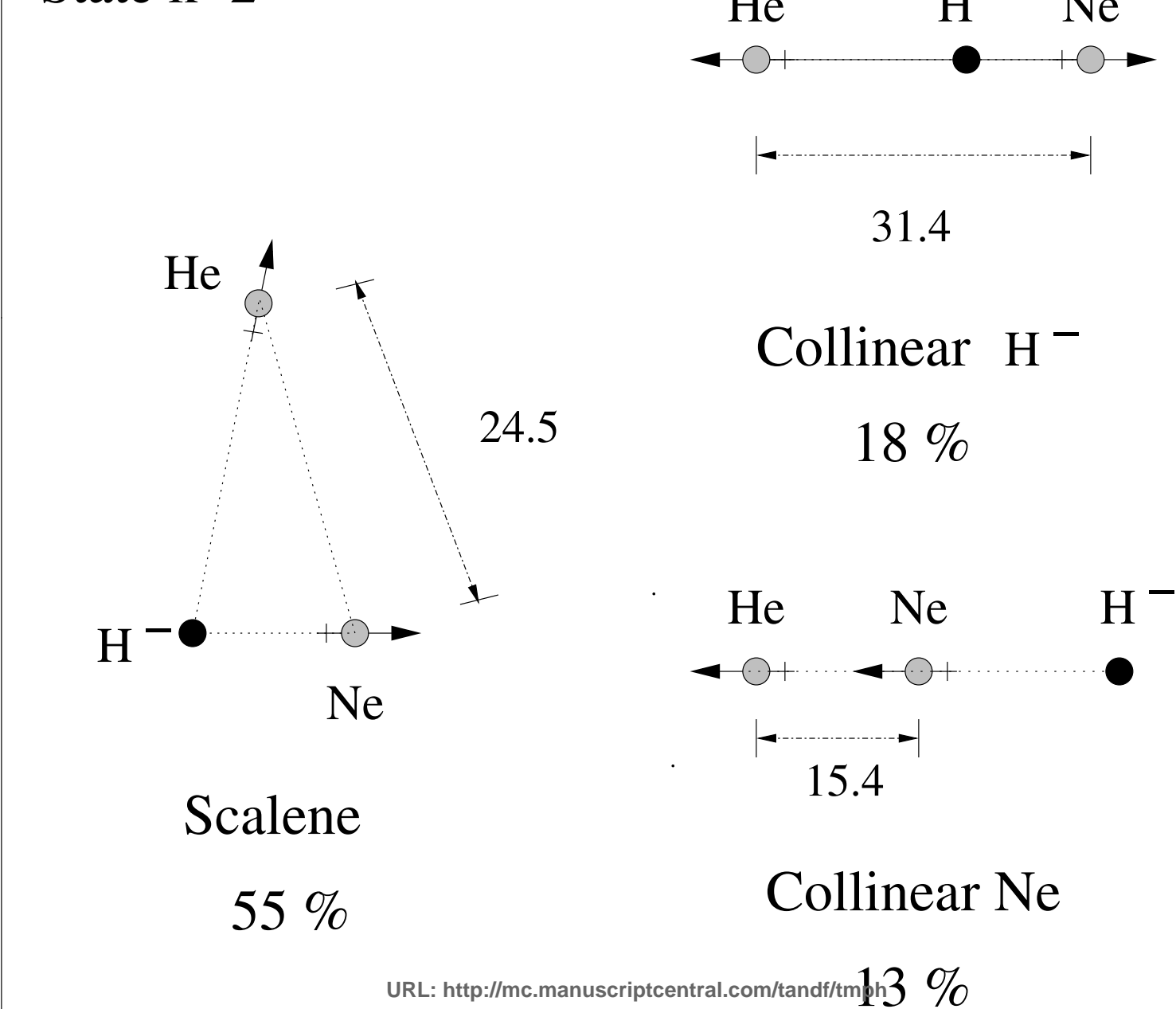
15 16 **Acknowledgments**

17
18 We thank the University of Rome Research Committee, the EU Network HPRN-CT-
19 2002-00290 and the INTAS project no. 03-51-6170 for supporting the present research. The
20 CASPUR Computing Consortium is also warmly thanked for its support.
21
22
23
24
25
26
27
28
29
30
31
32
33
34
35
36
37
38
39
40
41
42
43
44
45
46
47
48
49
50
51
52
53
54
55
56
57
58
59
60

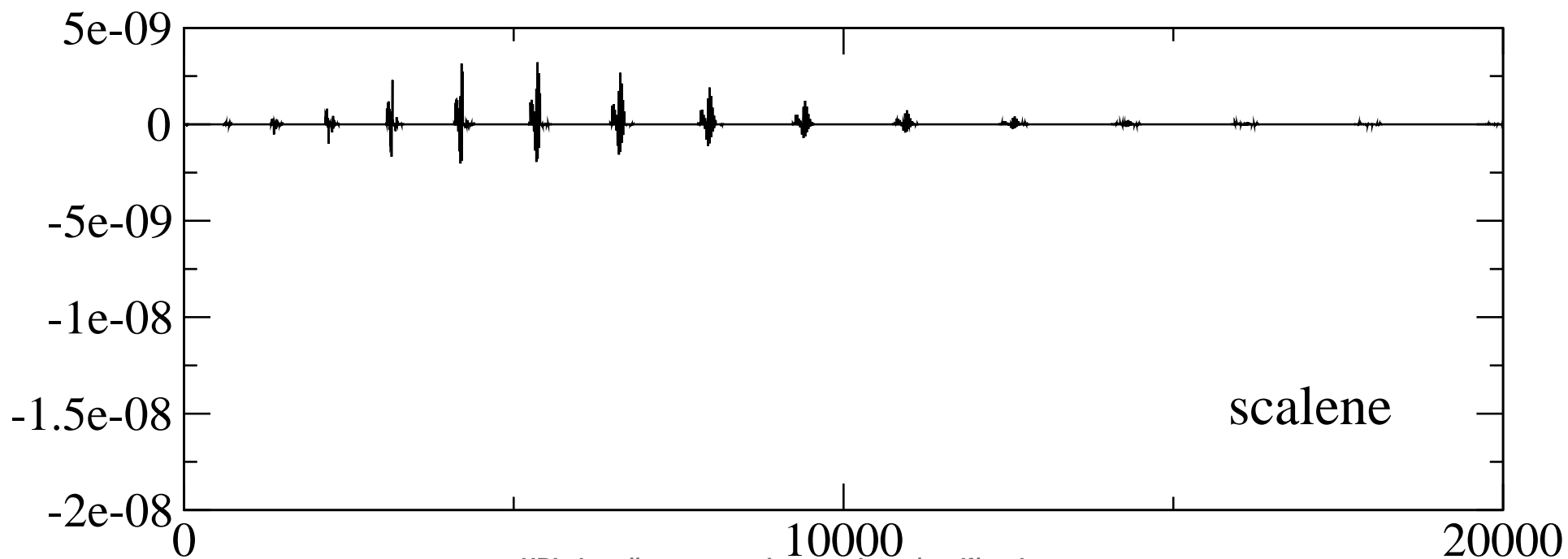
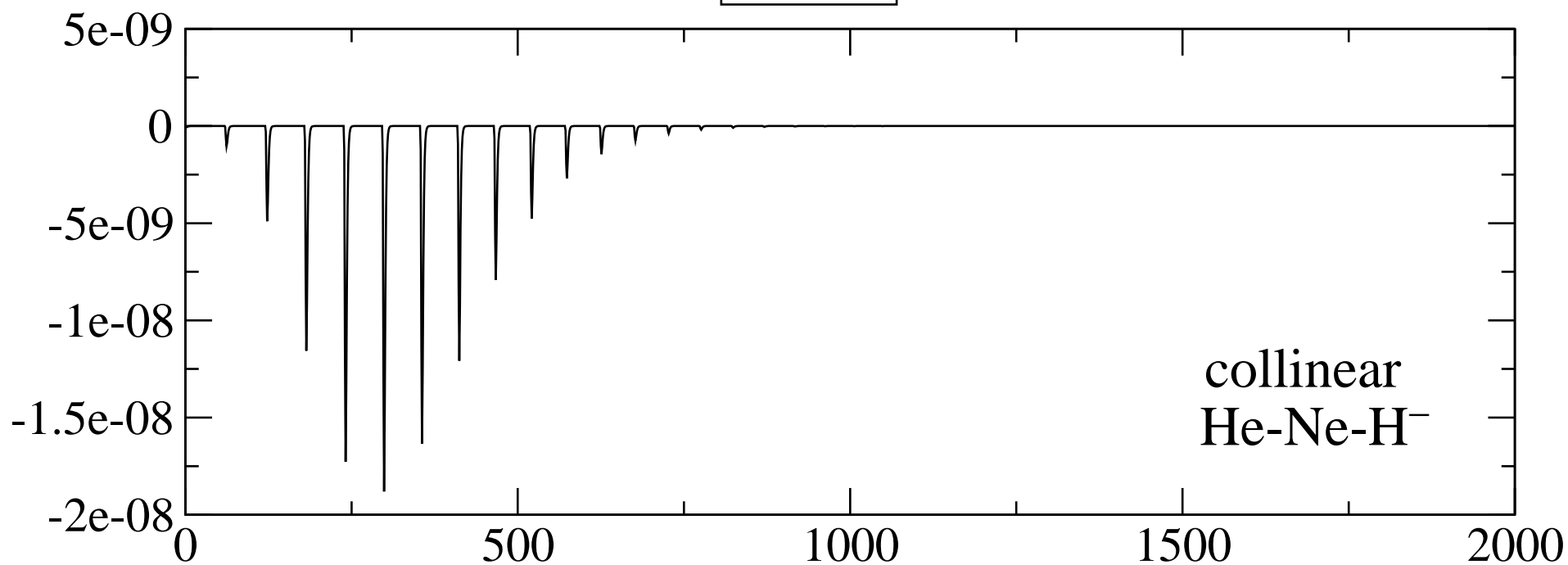
-
- 1
2
3
4
5
6
7 [1] L.H. Thomas, Phys. Rev. A **47**, 903 (1935).
8
9 [2] V. Efimov, Phys. Lett. **33B**, 563 (1970).
10
11 [3] C.A. Regal, C. Ticknor, J.L. Bohn and D.S. Jin, Nature **424**, 47 (2003).
12
13 [4] K.E. Strecker, G.B. Partridge and R.G. Hulet, Phys. Rev. Lett. **91**, 080406 (2003).
14
15 [5] J. Herbig, T. Kraemer, M. Mark, T. Weber, C. Chin, H.-C. Naegerl and R. Grimm, Science
16 **301**, 1510 (2003).
17
18 [6] S. Dürr, T. Valz, A. Marte and G. Rempe, Phys. Rev. Lett. **92**, 020406 (2004).
19
20 [7] S.T. Thompson, E. Hodby and A.E. Wieman, Phys. Rev. Lett. **94**, 020401 (2005).
21
22 [8] e.g. see: E. Braaten and H.-W. Hammer, Annals of Physics **8322**, 120 (2007).
23
24 [9] T. Gonzalez-Lezána, J. Rubajo-Soneira, S. Miret-Artès, F.A. Gianturco, G. Delgado-Barrio
25 and P. Villarreal, Phys. Rev. Lett. **82**, 1648 (1999); J. Chem. Phys, **110**, 9000 (1999).
26
27 [10] F.A. Gianturco, I. Baccarelli, T. Gonzalez-Lezána, S. Miret-Artès, G. Delgado-Barrio and P.
28 Villarreal, Europhys Lett. **50**, 567 (2000).
29
30 [11] T. Gonzalez-Lezána, S. Miret-Artès, G. Delgado-Barrio, P. Villarreal, J. Rubajo-Soneira, I.
31 Baccarelli and F.A. Gianturco, Phys. Rep. **452**, 1 (2007).
32
33 [12] I. Baccarelli, F.A. Gianturco, T. Gonzalez-Lezana, G. Delgado-Barrio, S. Miret-Artès and P.
34 Villarreal, J. Chem. Phys. **122**, 144319 (2005).
35
36 [13] F. Sebastianelli, I. Baccarelli, C. Di Paola and F.A. Gianturco, J. Chem. Phys. **119**, 5570
37 (2003).
38
39 [14] S. Orlandini, I. Baccarelli and F.A. Gianturco, J. Chem. Phys. **125**, 234307 (2006).
40
41 [15] I.P. Hamilton and J.C. Light, J. Chem. Phys. **84**, 306 (1986).
42
43 [16] G.L.G Sleijpen and H.A. van der Vorst, SIAM J. Mat. Anal and Appl., **17**, 401 (1996).
44
45 [17] C. Di Paola, F.A. Gianturco, G. Delgado-Barrio, S. Miret-Artès, P. Villarreal and I. Baccarelli,
46 Collect. Czech Chem. Comm. **151**, 187 (2003).
47
48 [18] I. Baccarelli, F.A. Gianturco, T. Gonzalez-Lezana, G. Delgado-Barrio, S. Miret-Artès and P.
49 Villarreal, J. Chem. Phys. **122**, 084313 (2005).
50
51 [19] Y.D. Liu, P.N. Roy, J. Chem. Phys. **121**, 6282 (2004).
52
53 [20] K.T. Tang and J.P. Toennies, J. Chem. Phys. **118**, 4976 (2003).
54
55 [21] D. Cvetko, A. Lansì, A. Morgante, F. Tommasini, P. Cortona, M.G. Dondi, J. Chem. Phys.
56
57
58
59
60

- 1
2
3
4
5
6
7
8
9
10
11
12
13
14
15
16
17
18
19
20
21
22
23
24
25
26
27
28
29
30
31
32
33
34
35
36
37
38
39
40
41
42
43
44
45
46
47
48
49
50
51
52
53
54
55
56
57
58
59
60
- 100**, 2052 (1994).
- [22] C. Di Paola, F.A. Gianturco, F. Paesani, G. Delgado-Barrio, S. Miret-Artès, P. Villarreal, I. Baccarelli and T. González-Lezana, *J. Phys. B* **35**, 2643 (2002).
- [23] G.L. Bendazzoli, S. Evangelisti and F. Passarini, *Chem. Phys.* **215**, 217 (1997).
- [24] e.g. see: R.J. Bell and I.J. Zucker, in *Rare Gas Solids*, edited by M.L. Klein and J.A. Venables, Academic, London (1976).
- [25] B.M. Axilrod and E. Teller, *J. Chem. Phys.* **11**, 299 (1943).
- [26] A. Kumar and W. Meath, *Can. J. Chem.* **63**, 1616 (1985).
- [27] A.J. Stone, *The Theory of Intermolecular Forces*, Clarendon Press, Oxford (1996).
- [28] B.D. Esry, C.D. Lin and C.H. Greene, *Phys. Rev. A* **54**, 394 (1996).
- [29] S. Geltman, *Mol. Phys.* **105**, 1971 (2007).
- [30] R. Bruhl, A. Kalinin, O. Kornilov, J. P. Toennies, G. C. Hegerfeldt and M. Stoll *Phys. Rev. Lett.* **95**, 063002 (2005).
- [31] T. Kraemer, M. Mark, P. Waldburger, J.G. Danzl, C. Chin, B. Engeser, A.D. Lange, K. Pilch, A. Jaakkala, H.-C. Naegerl and R. Grimm, *Nature* **440**, 315 (2006).

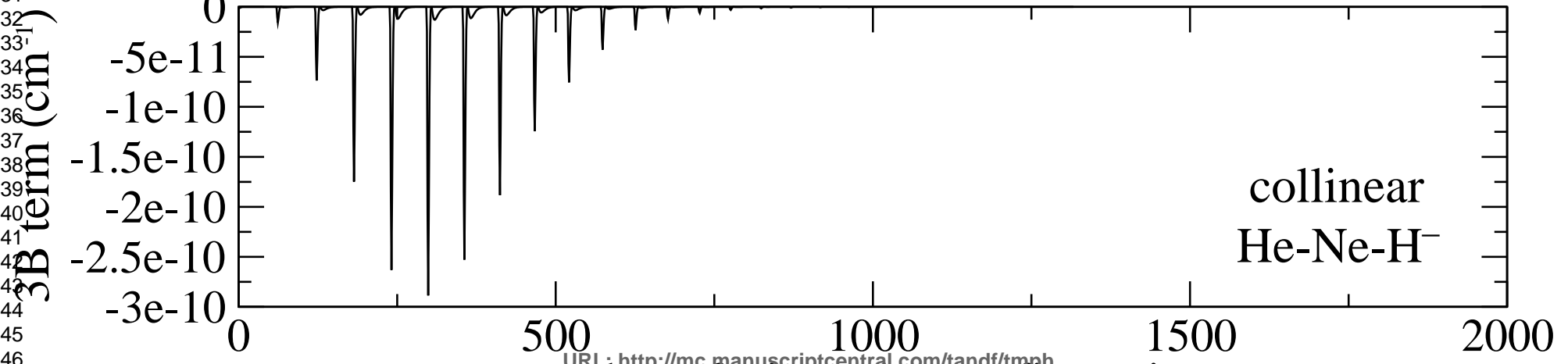
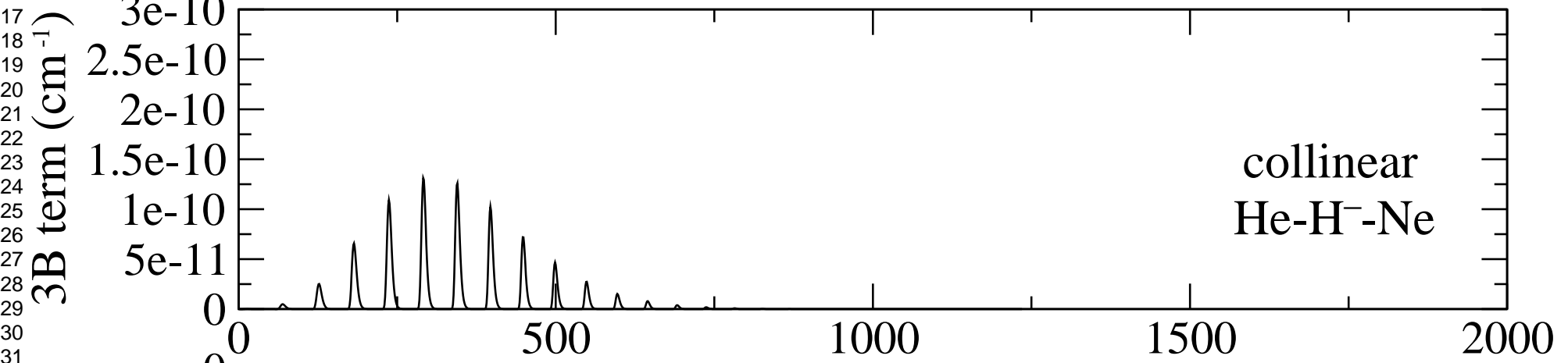
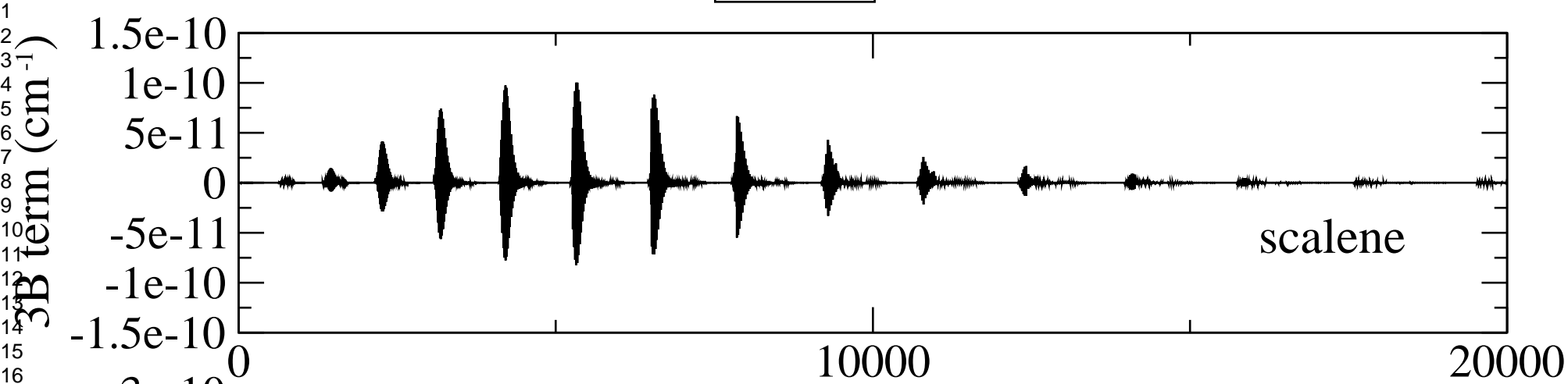


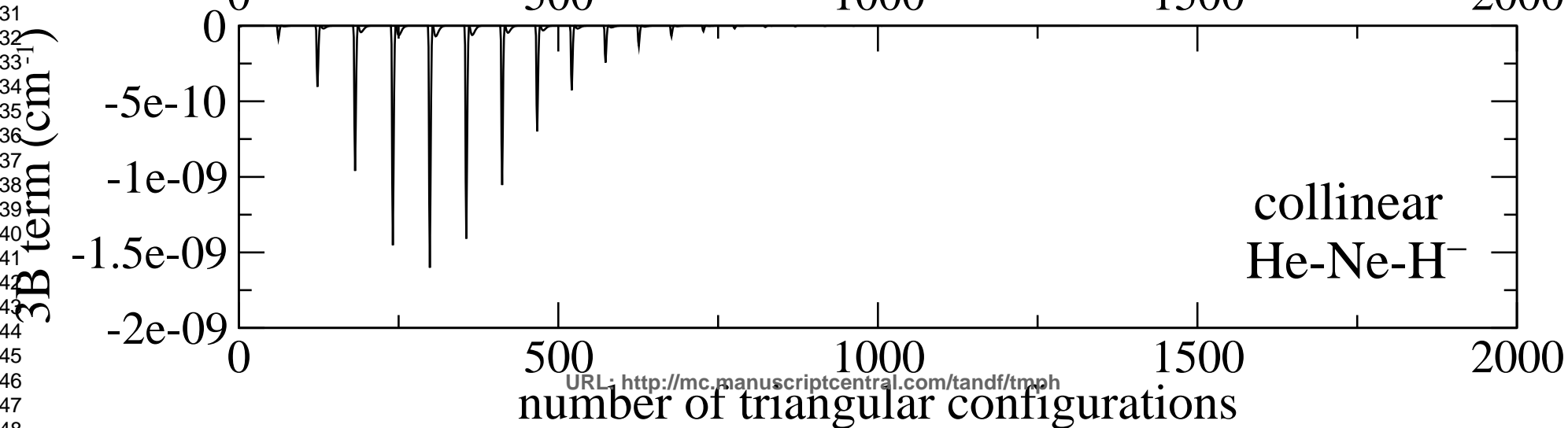
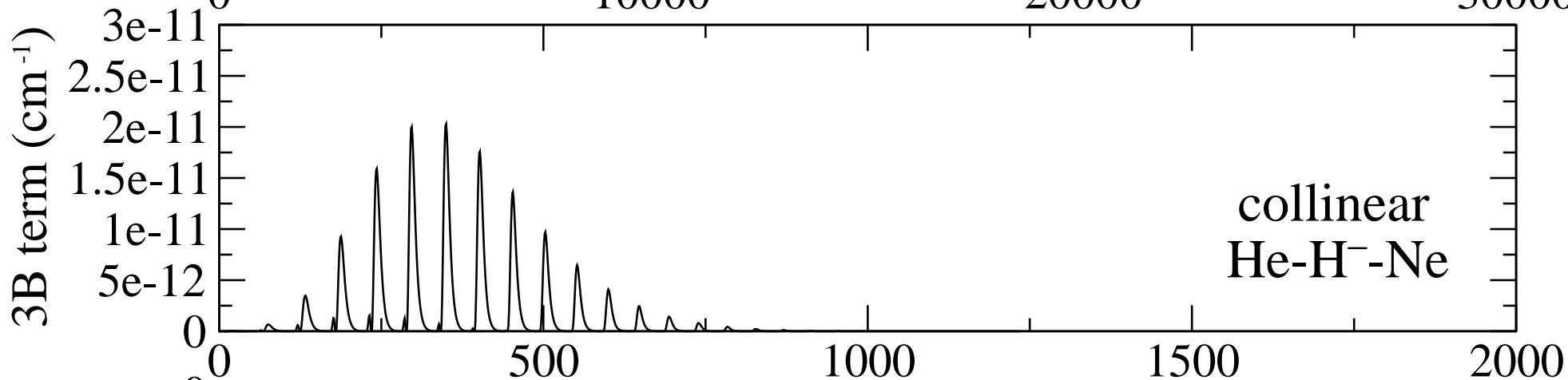
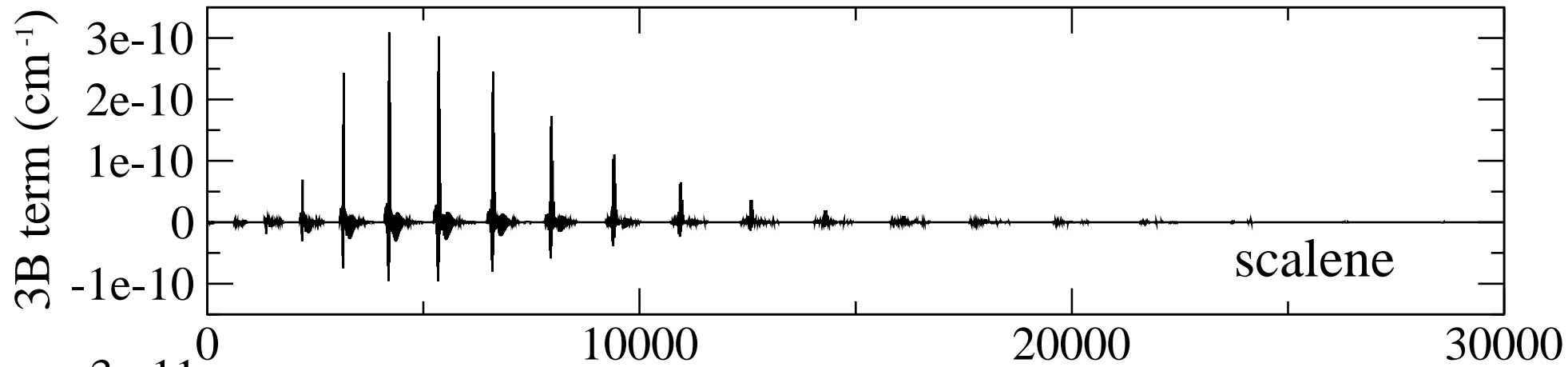
State $k=0$ State $k=1$ State $k=2$ 

$$k = 0$$



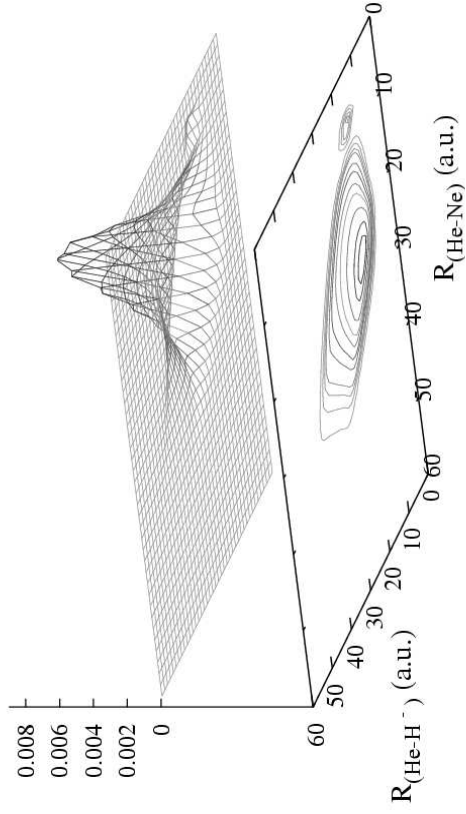
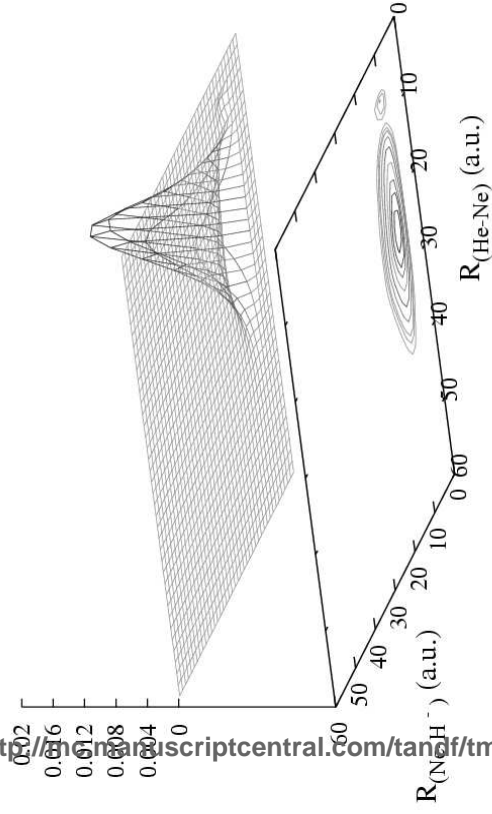
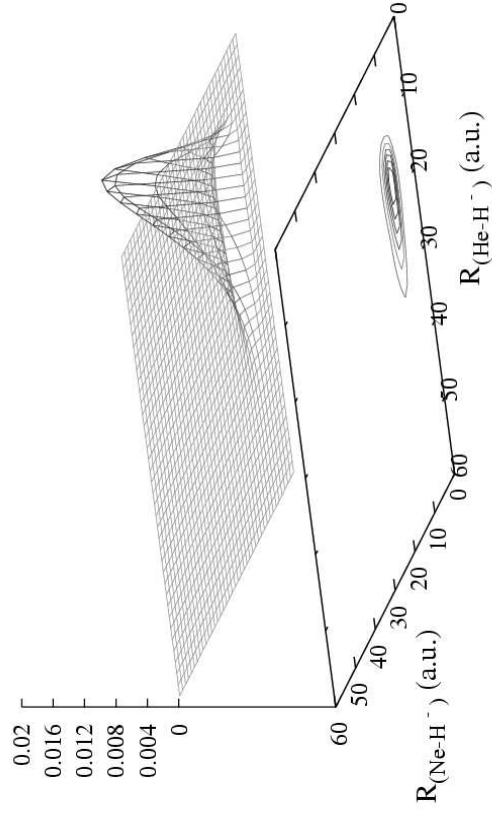
Molecular Physics
 $k = 1$



$k = 2$ 

1
2
3
4
5
6
7
8
9
10
11
12
13
14
15
16
17
18
19
20
21
22
23
24
25
26
27

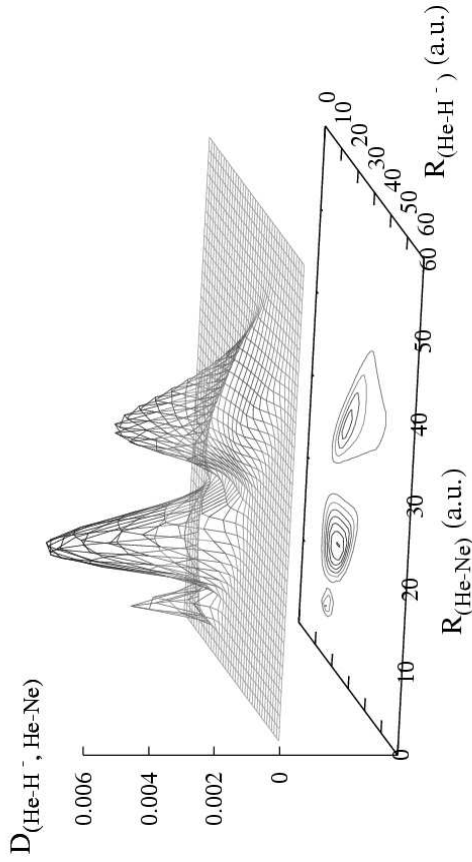
2D distributions

 $D_{(\text{He-H}^-, \text{He-Ne})}$  $D_{(\text{Ne-H}^-, \text{He-Ne})}$  $D_{(\text{Ne-H}^-, \text{He-H}^-)}$ 

URL: <http://mc.manuscriptcentral.com/tandf/tpmh>

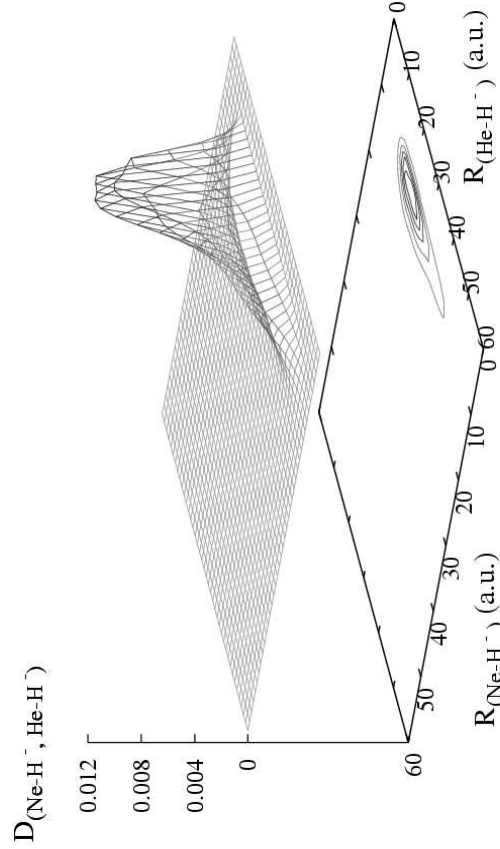
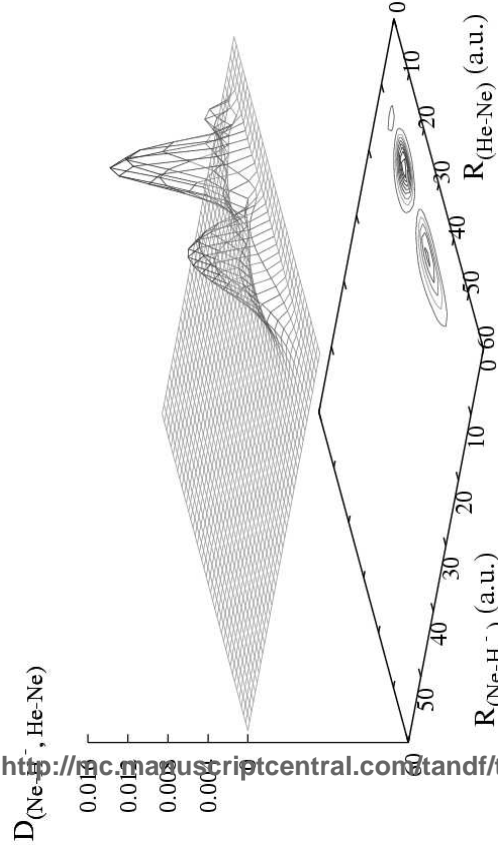
1
2
3
4
5
6
7
8
9
10
11
12
13
14
15
16
17
18
19
20
21
22
23
24
25
26
27

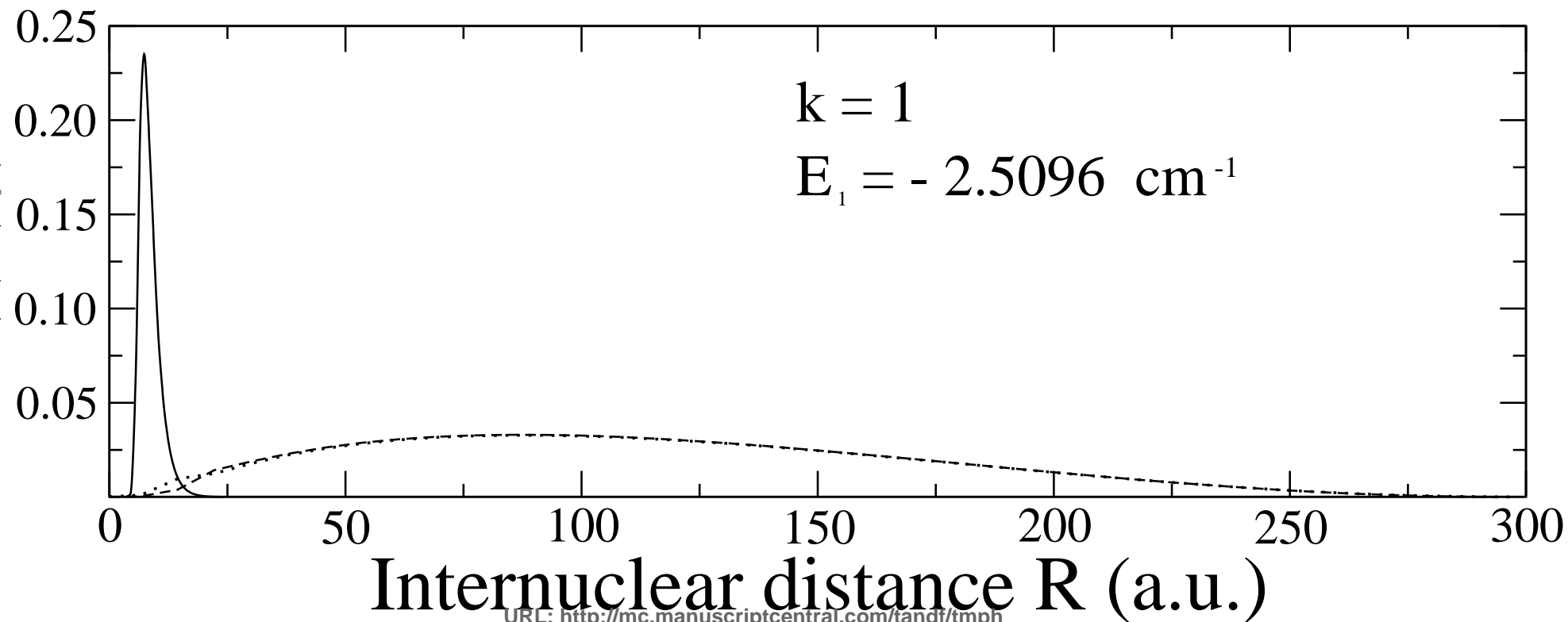
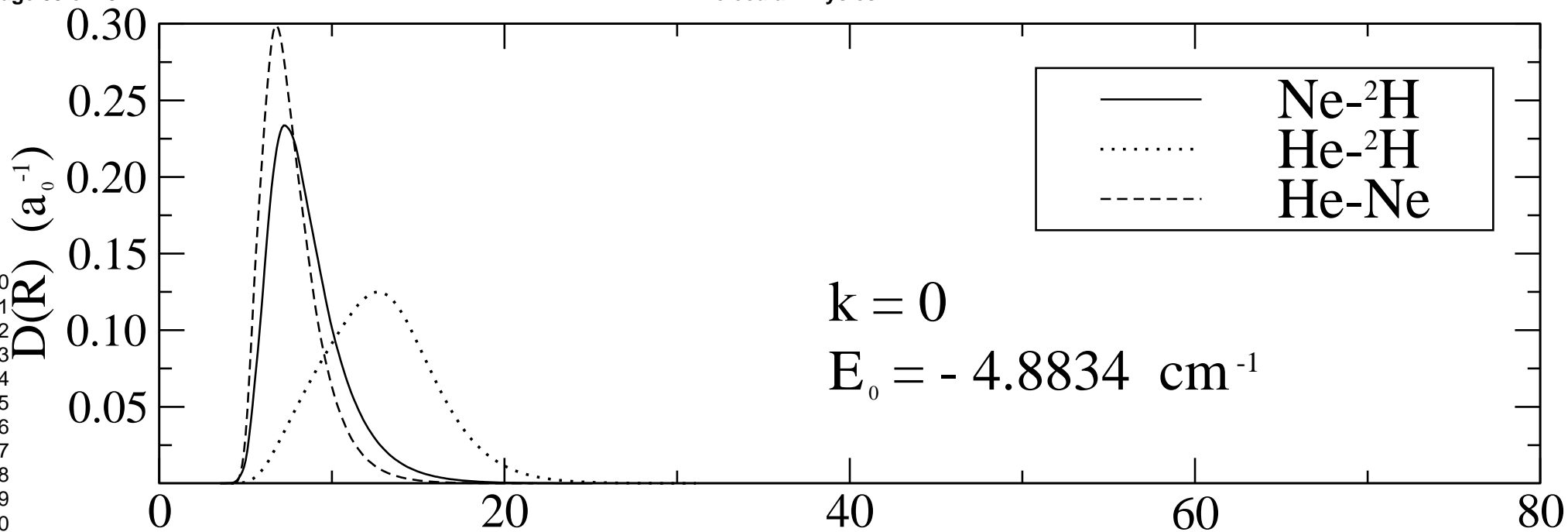
2D distributions

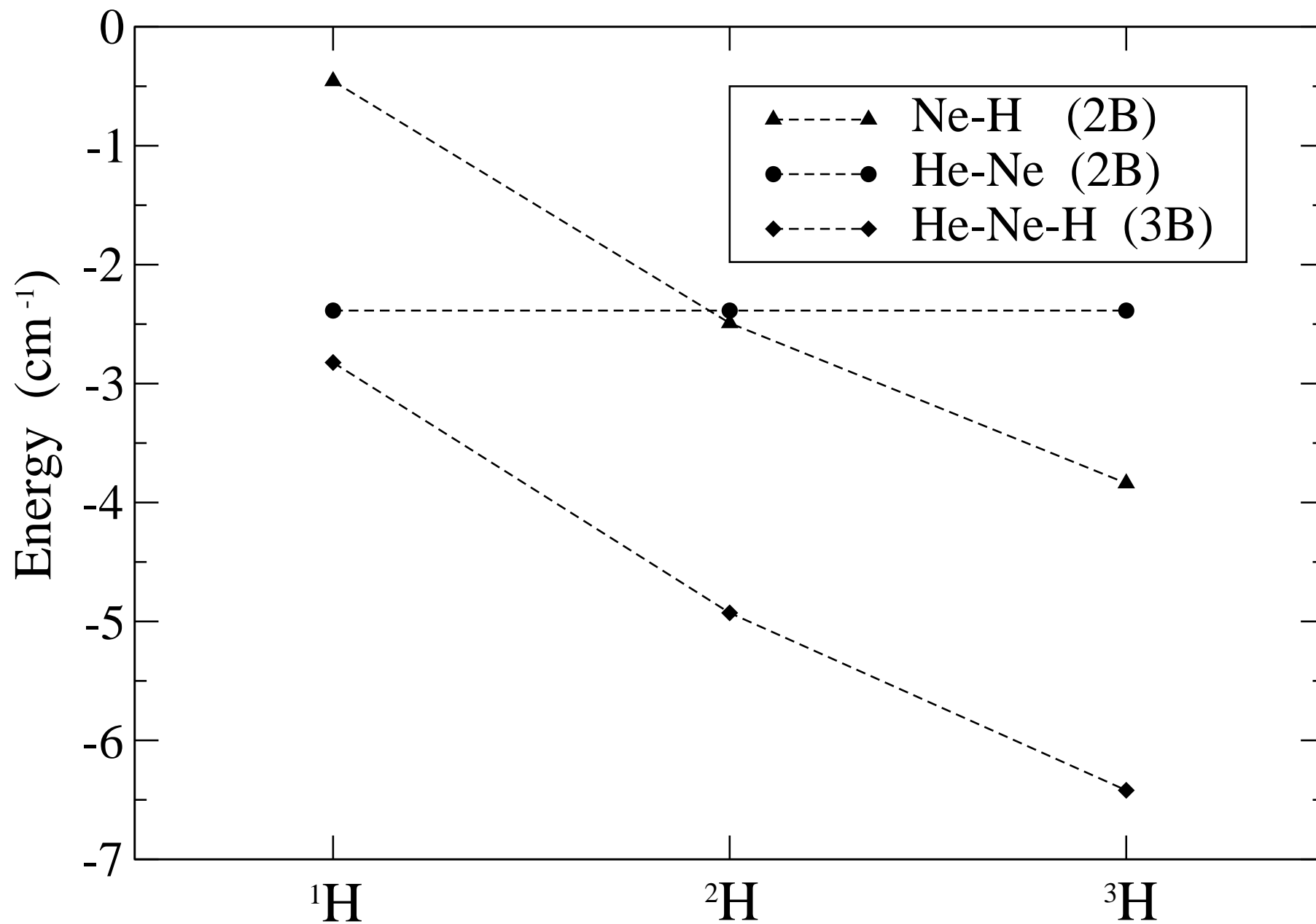


URL: <http://mc.manuscriptcentral.com/standf/tpmh>

Molecular Physics



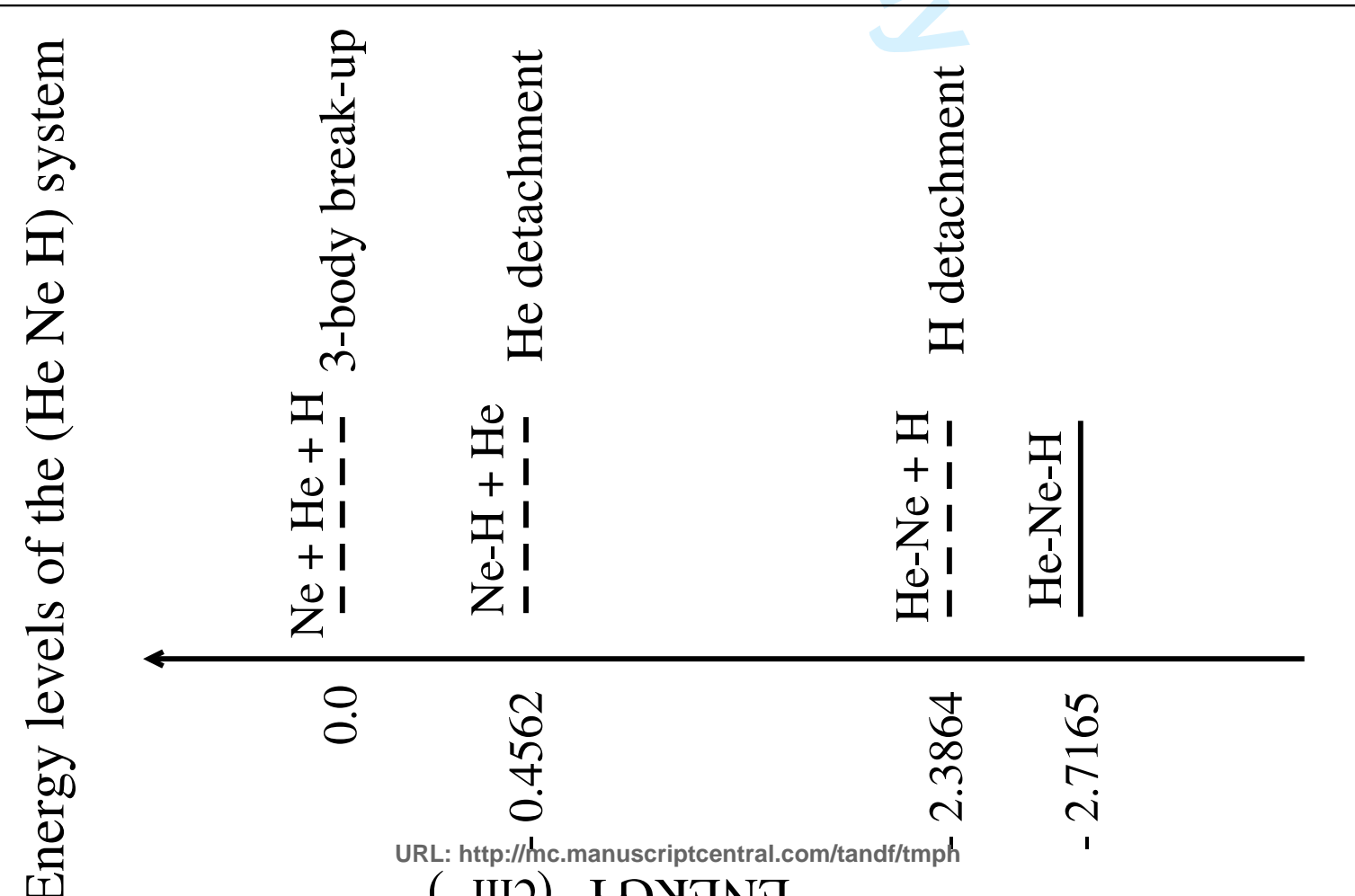
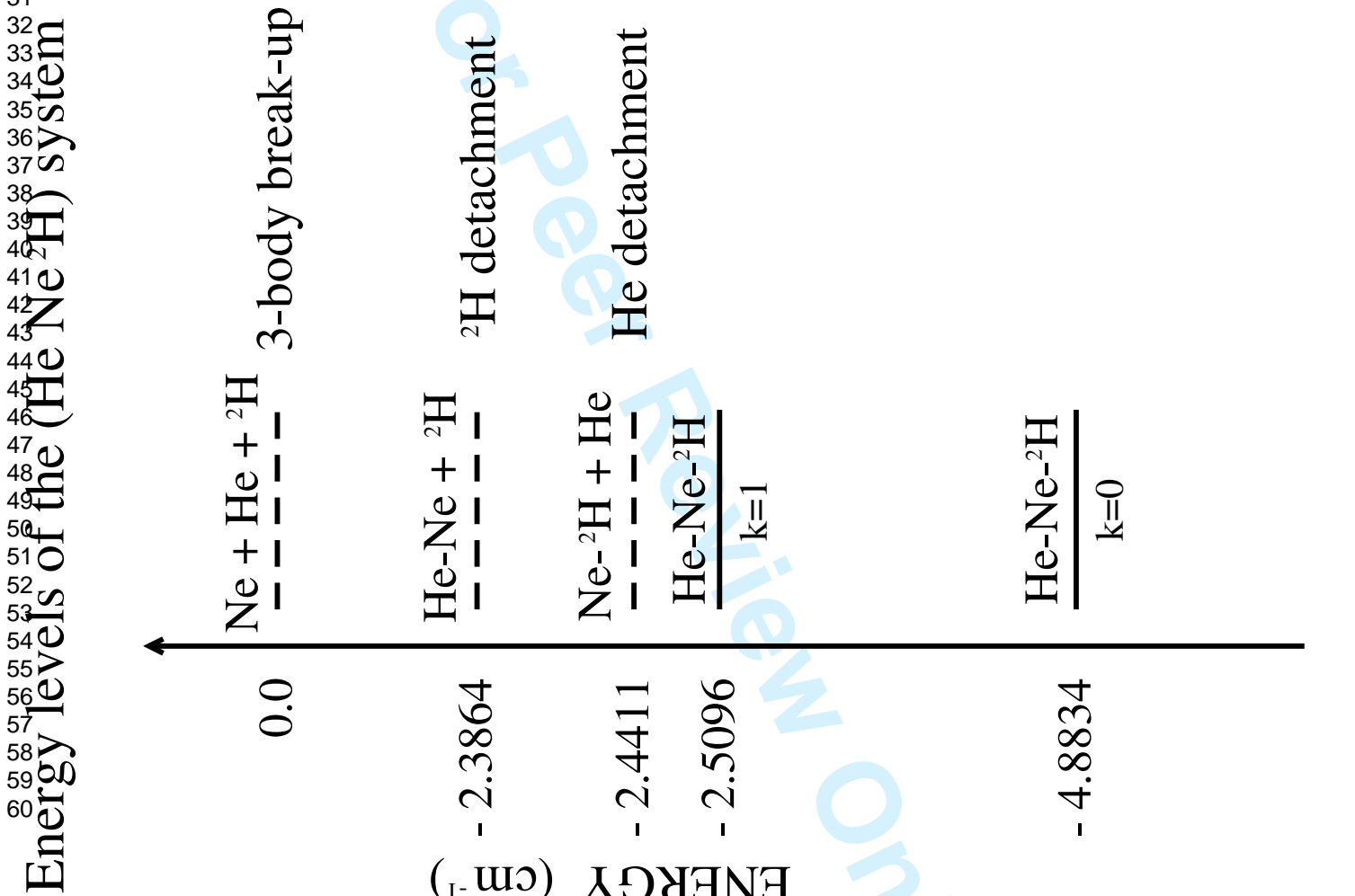
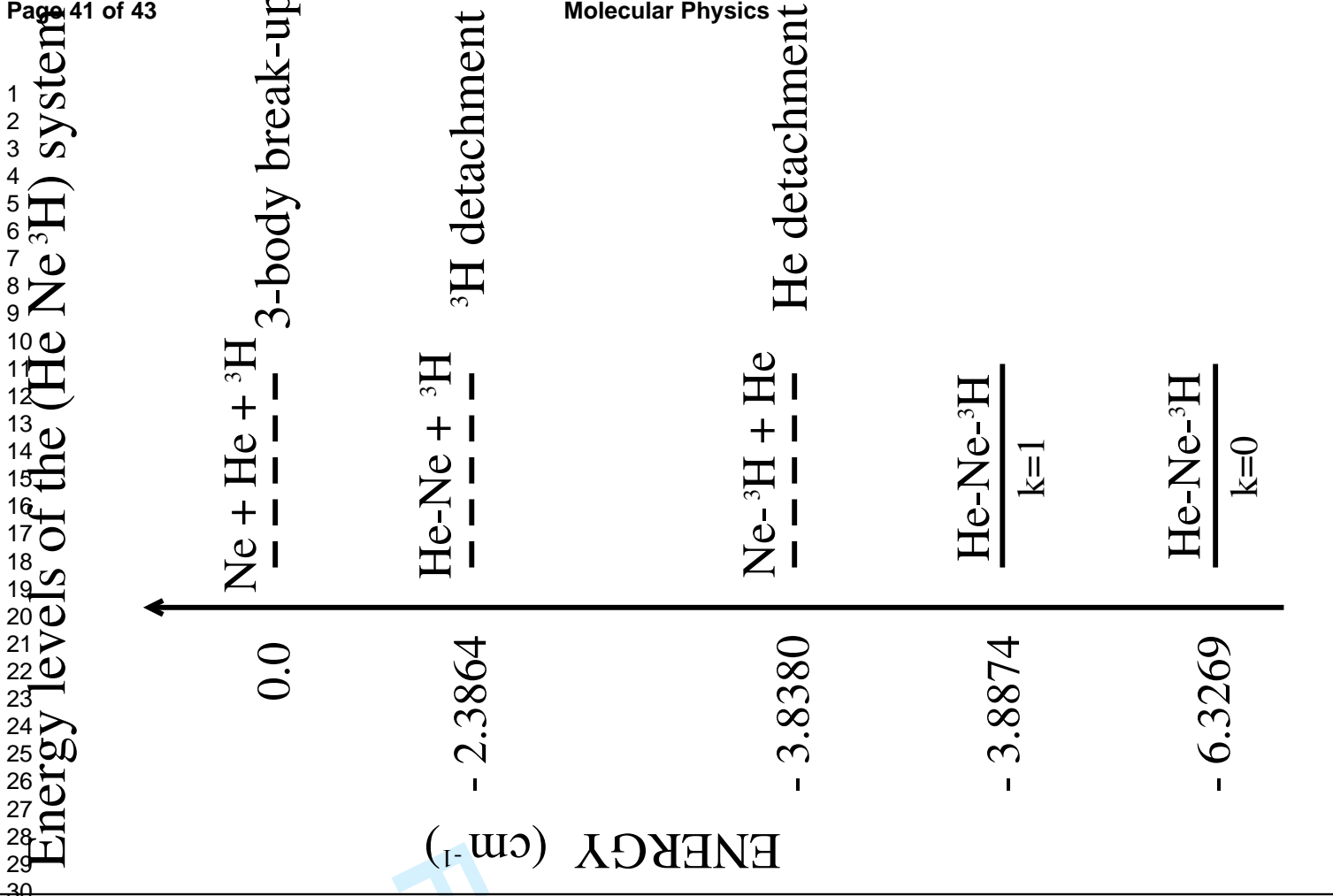
1
2
3
4
5
6
7
8
9
10
11
12
13
14
15
16
17
18
19
20
21
22
23
24
25
26
27
28
29
30
31
32
33
34
35
36
37
38
39
40
41
42
43
44
45
46
47
48
49



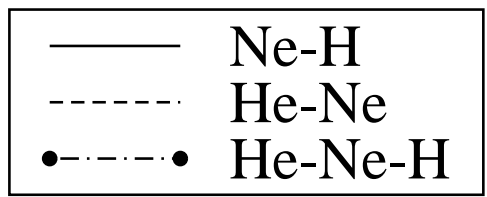
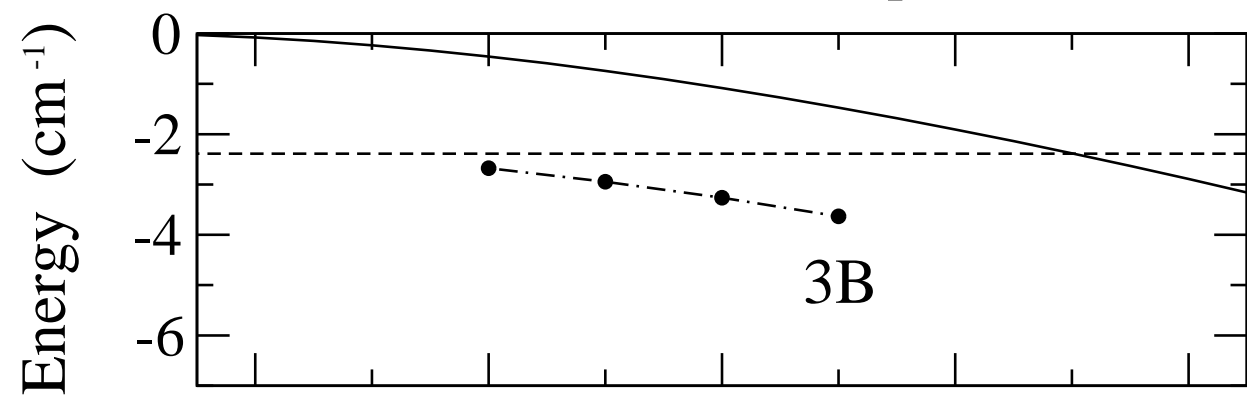
Energy levels of the (He Ne ³H) system

Energy levels of the (He Ne ²H) system

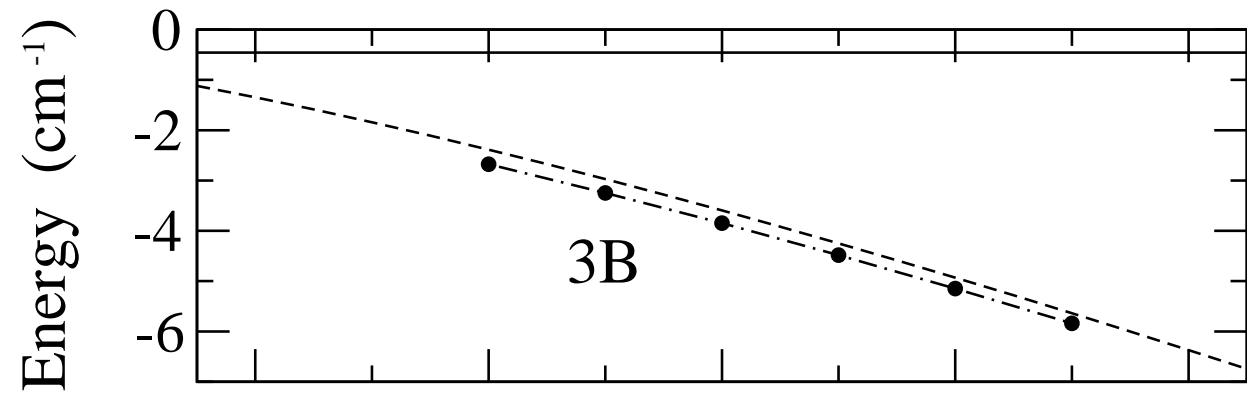
Energy levels of the (He Ne H) system



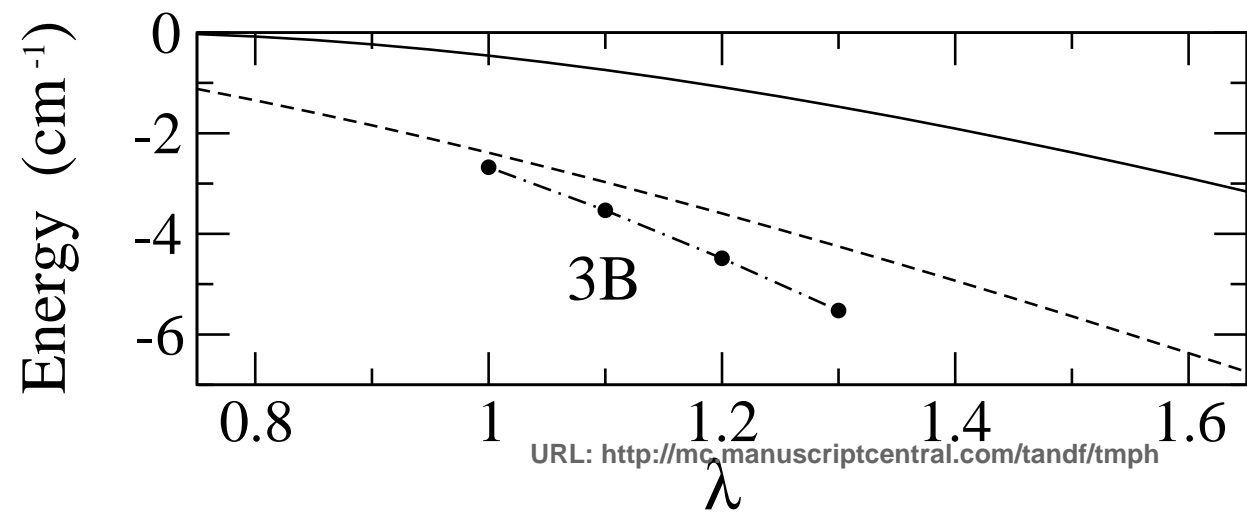
Variation of the Ne-H potential



Variation of the He-Ne potential

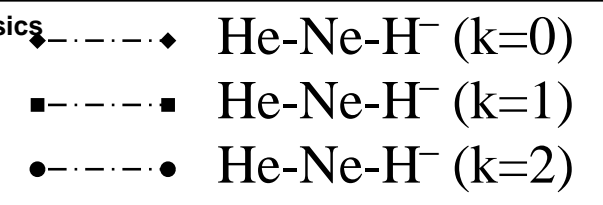
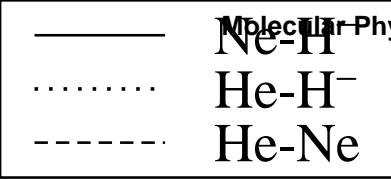


Variation of all the 2B-potentials



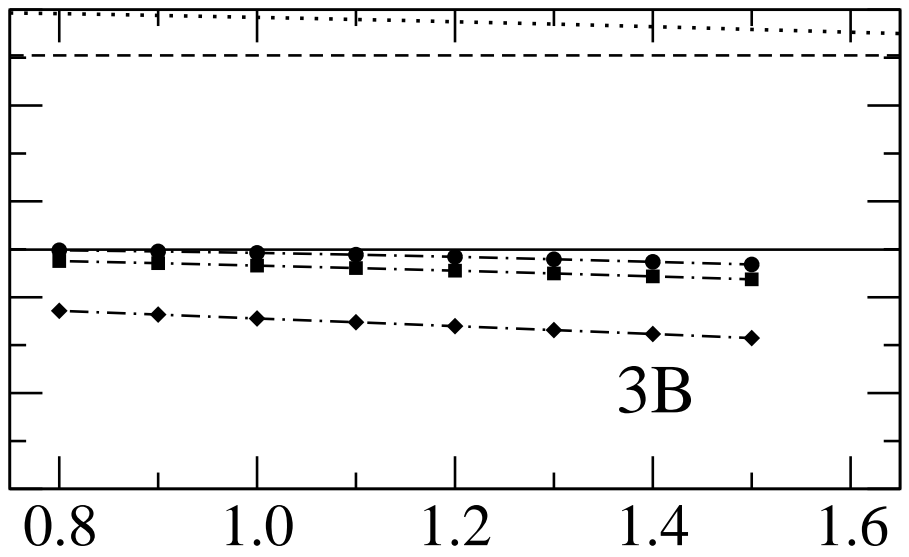
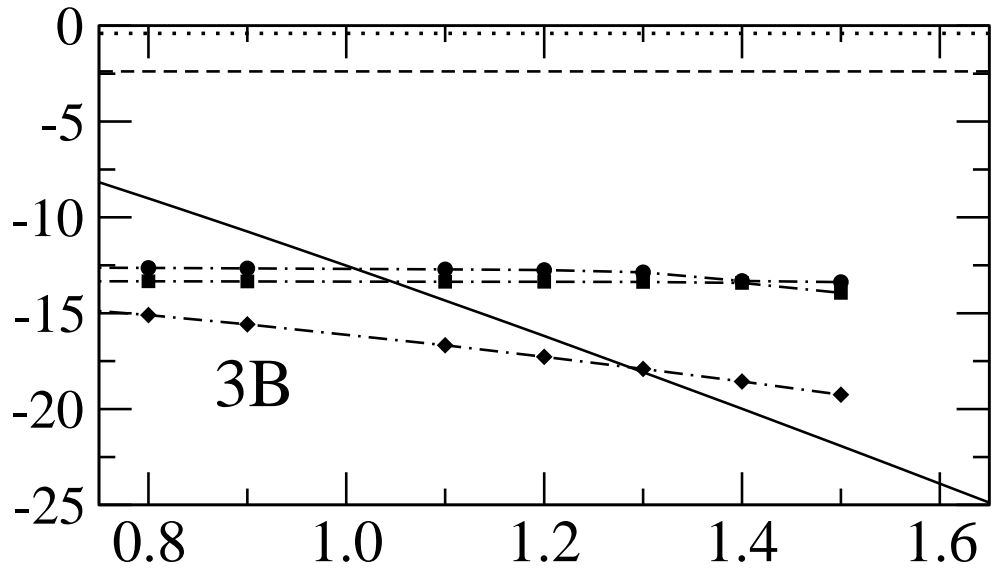
λ

1
2
3
4
5
6
7
8
9
10
11
12
13
14
15
16
17
18
19
20
21
22
23
24
25
26
27
28
29
30
31
32
33
34
35
36
37
38
39
40
41
42
43
44
45
46
47
48
49



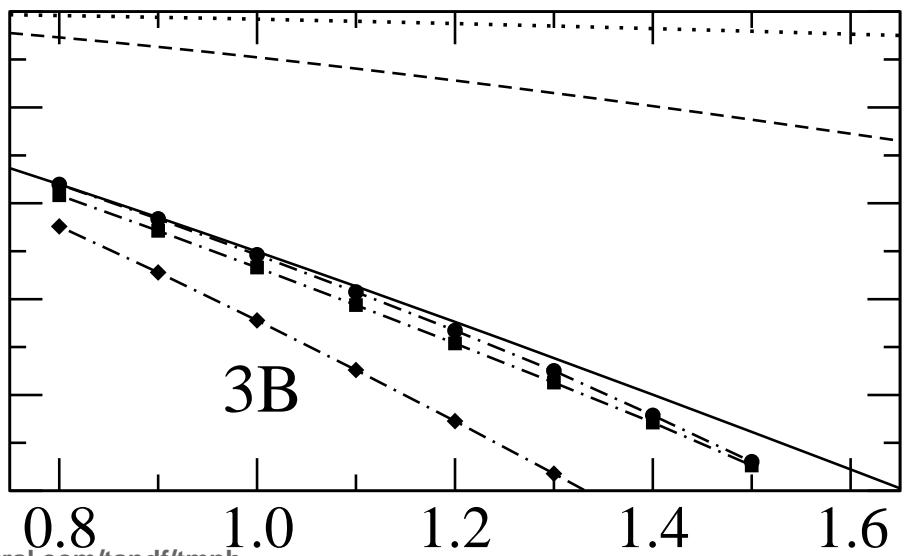
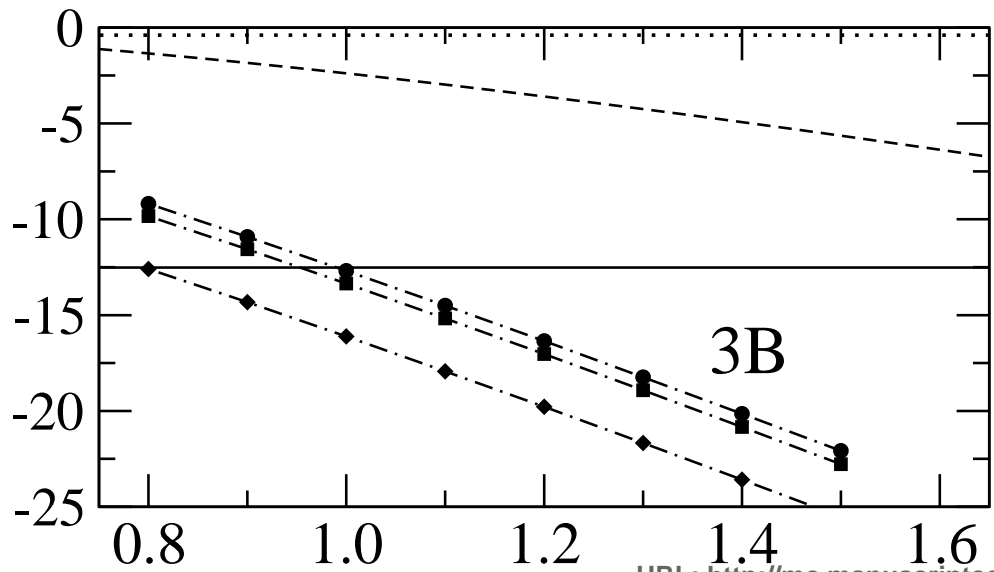
Variation of the Ne-H⁻ potential

Variation of the He-H⁻ potential



Variation of the He-Ne potential

Variation of all the 2B-potentials



1
2
3
4
5
6
7
8
9
10
11
12
13
14
15
16
17
18
19
20
21
22
23
24
25
26
27
28
29
30
31
32
33
34
35
36
37
38
39
40
41
42
43
44
45
46
47
48
49